NASA CR-152124
March 1978

Flap Survey Test of a Combined Surface Blowing Model

Flow Measurements at Static Flow Conditions

By
Toshiyuki Fukushima

Prepared under Contract No. NAS2-9693
by
Boeing Vertol Company
Philadelphia, Pennsylvania
for

NASA

National Aeronautics and
Space Administration

Ames Research Center
Moffett Field, California

NASA CR-152124
March 1978

FLAP SURVEY TEST OF A COMBINED SURFACE BLOWING MODEL FLOW MEASUREMENTS AT STATIC FLOW CONDITIONS

By
Toshiyuki Fukushima

Prepared under Contract No. NAS2-9693 by
Boeing Vertol Company
Philadelphia, Pennsylvania

for

NATIONAL AERONAUTICS AND SPACE ADMINISTRATION

"Page missing from available version"

SUMMARY

The Combined Surface Blowing (CSB) V/STOL lift/ propulsion system consists of a blown flap system which deflects the exhaust from a turbojet engine over a system of flaps deployed at the trailing edge of the wing. The CSB system jet flows over both the upper and lower surfaces of the flaps. The particular model tested deployed triple-slotted flaps.

This test was a sequel to a previous performance test and the purpose was to locate and measure the sources of losses which limited the thrust recovery to a value of 0.9. The measurements were to be used to recommend changes to the system to improve its performance and to set the possible limits to the performance. Flow measurements consisting of velocity measurements using split film probes and total measure surveys using a miniature Kiel probe were made at control stations along the flap systems at two spanwise stations, the centerline of the nozzle and 60 percent of the nozzle span outboard of the centerline. Surface pressure measurements were made in the wing cove and the upper surface of the first flap element.

The test showed a significant flow separation in the wing cove. The extent of the separation is so large that the flow into the first flap takes place only at the leading edge of the flap. The velocity profile measurements indicate that large spanwise (3-dimensional) flow may exist. An attempt to measure the spanwise flow with the split film probe was unsuccessful, i.e., the probe was broken by the lateral force from the main chordwise flow.

ACKNOWLEDGMENT

This program was funded under Contract No. NAS2-9693 by NASA Ames Research Center. The NASA technical monitor was David G. Koenig.

TABLE OF CONTENTS

LIST OF ILLUSTRATIONS

LIST OF SYMBOLS

K	constant in Kiel probe calibration
m	exponent in Kiel probe calibration equation
P_T	measured static pressure
P_L	local static (ambient) pressure, tunnel ambient pressure
P_O	static (stagnation) pressure
WSTA	wing station measured from side of original fuselage, inches
θ	flow angularity for Kiel probe, degrees

1.0 INTRODUCTION

1.1 Background

The Combined Surface Blowing (CSB) system has been proposed as a V/STOL propulsion system which does not require the vectoring of the propulsion device and utilizes the known technology of flaps for vectoring the available thrust to achieve its V/STOL capability. The thrust vectoring is attained with certain losses inherent to the concept: i.e., turning, separation, slot flow, etc. Losses in the flow from the nozzle exit to the trailing edge of the last flap element decrease the velocity at the trailing edge of the deflected flaps and reduce the vertical thrust.

The tests reported in reference 1 show that flap configuration B gave the best performance with a thrust recovery of 0.89 at a nozzle pressure ratio of 1.2. The thrust recovery was nearly constant at this level between pressure ratio 1.05 and 1.2 and showed only a 2-percent decrease as the pressure ratio was increased to 1.4. This test is an attempt to apportion the causes of the 11-percent loss of thrust.

1.2 Objective

A prerequisite for improving the performance of the CSB system is to determine where the losses occur and the mechanism of the losses so that changes can be incorporated. The measurements required to accomplish this were chosen to be the velocities and flow angularities and the total pressure at selected chordwise stations along the nozzle centerline and at an outboard station 2 inches inboard of the flap bracket so that the flow was inside of the bracket.

1.3 Scope

A one-week test was conducted from September 12 to 19, 1977, in the Boeing Vertol V/STOL wind tunnel. Sixty-five wind-off test runs were made with a half-span model with an air pod and nozzle and triple-slotted trailing-edge flaps. Figures 1-1 and 1-2 show the model in the wind tunnel working section. One wing length and spanwise pod location were tested, similar to the extended wing of reference 1 but with the half body removed to permit traversing of probes. All tests were performed with the one flap configuration, using settings obtained from the earlier test. One thrust level, comparable to 1.2 pressure ratio, was used for the investigation of losses.

Surface static pressures were measured at 10 chordwise locations in the flap cove and upper surface of the first flap segment at two spanwise locations. Hot film measurements were made at 12 or more chord locations at the two spanwise positions.

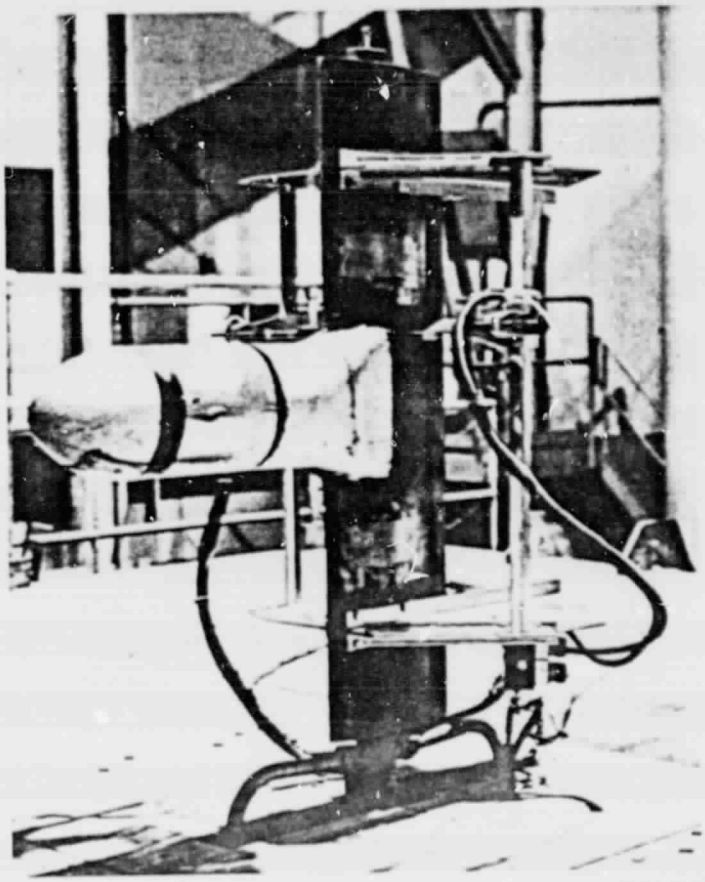

Figure 1–1. Three-quarter front view of test model showing upper surface of wing

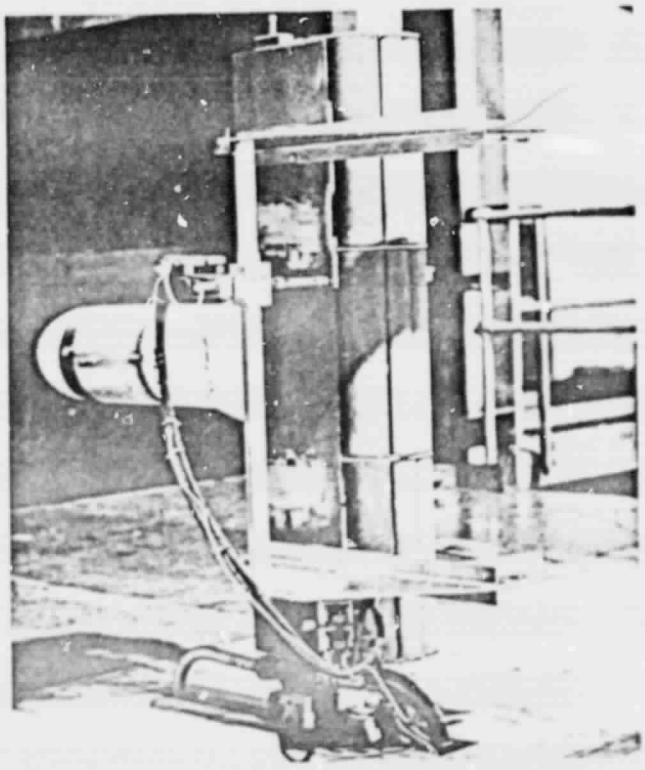

Figure 1–2. Three-quarter rear view of test model showing upper surface of wing and flaps

2.0 MODEL DESCRIPTION AND INSTALLATION

The general arrangement and geometry of the half-span model and the wind tunnel installation are presented in this section.

2.1 Wing Geometry

Figure 2-1 shows the wing planform geometry and nacelle location used throughout this test. Other details of wing geometry are listed below. This is the same as the extended wing of reference 1, with the half-body removed to facilitate traversing probes.

Wing Geometry

Chord	1.0715 ft
Taper	0.0
Span (2 x semispan, excluding round tip)	8.792 ft
Area (2 x reference area)	9.421 ft^2
Aspect ratio	8.205
Sweepback	0.0
Basic wing section	63_3418
Triple-slotted flap	41% wing chord retracted approx 9.5% Fowler action at 90°

The wing cross section and locations of nozzle exit and flap hinge are shown in Figure 2-2.

2.2 Flap Geometry

One flap geometry was used for all tests. The three-element flap included a large forward segment and two smaller-chord segments as shown in Figure 2-2. The gaps and slot geometry were selected on the basis of tests in reference 1 and were set at the values shown in Figure 2-3. Thrust calibrations were run with the flaps retracted. All other data runs were made with the 90-degree setting shown, which has an actual trailing-edge flap angle of 89 degrees.

There are three spanwise flap segments. They are basically equal in length, but the inner segment has been shortened by 0.02 foot. Each segment is assembled to the 90-degree setting and then bolted to the wing flap brackets.

No slats were used on the leading edge during this test.

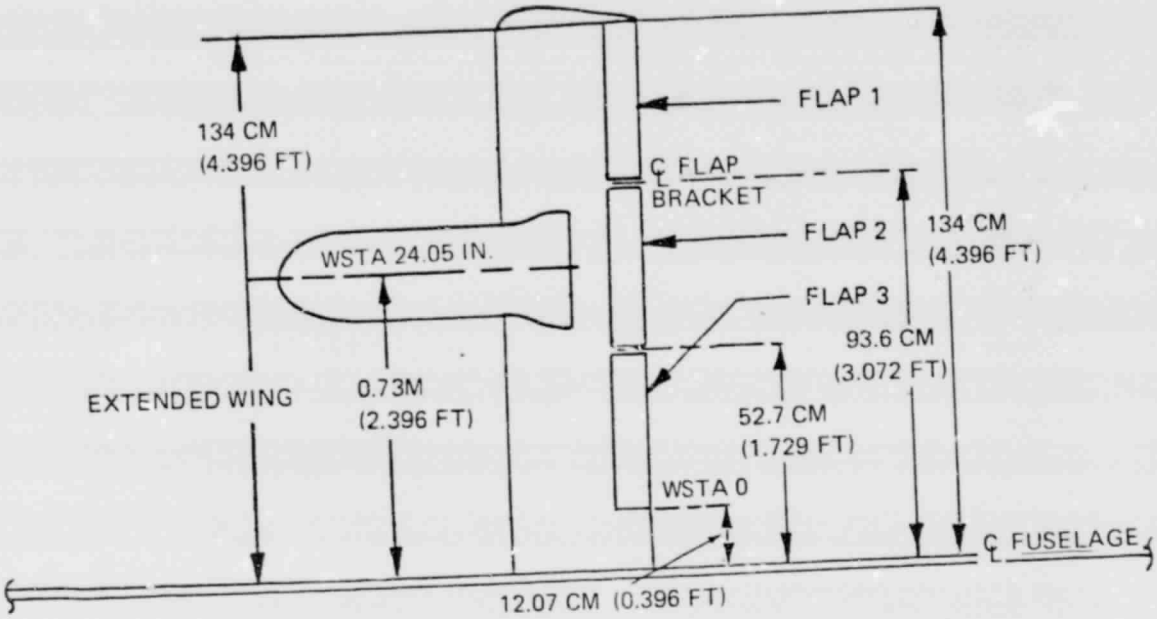

Figure 2–1. Combined surface blowing model

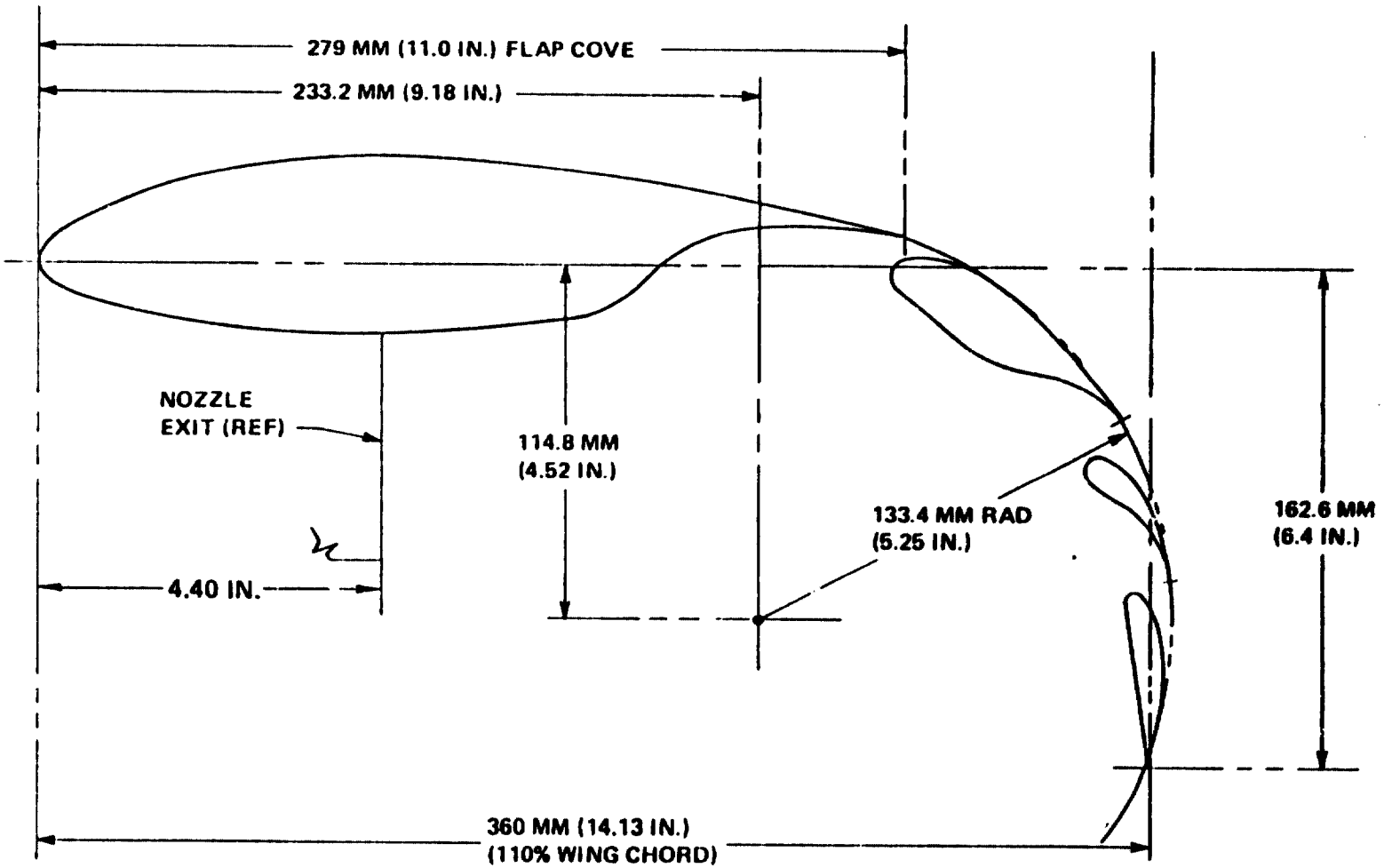

Figure 2–2. Wing and flaps in extended configuration

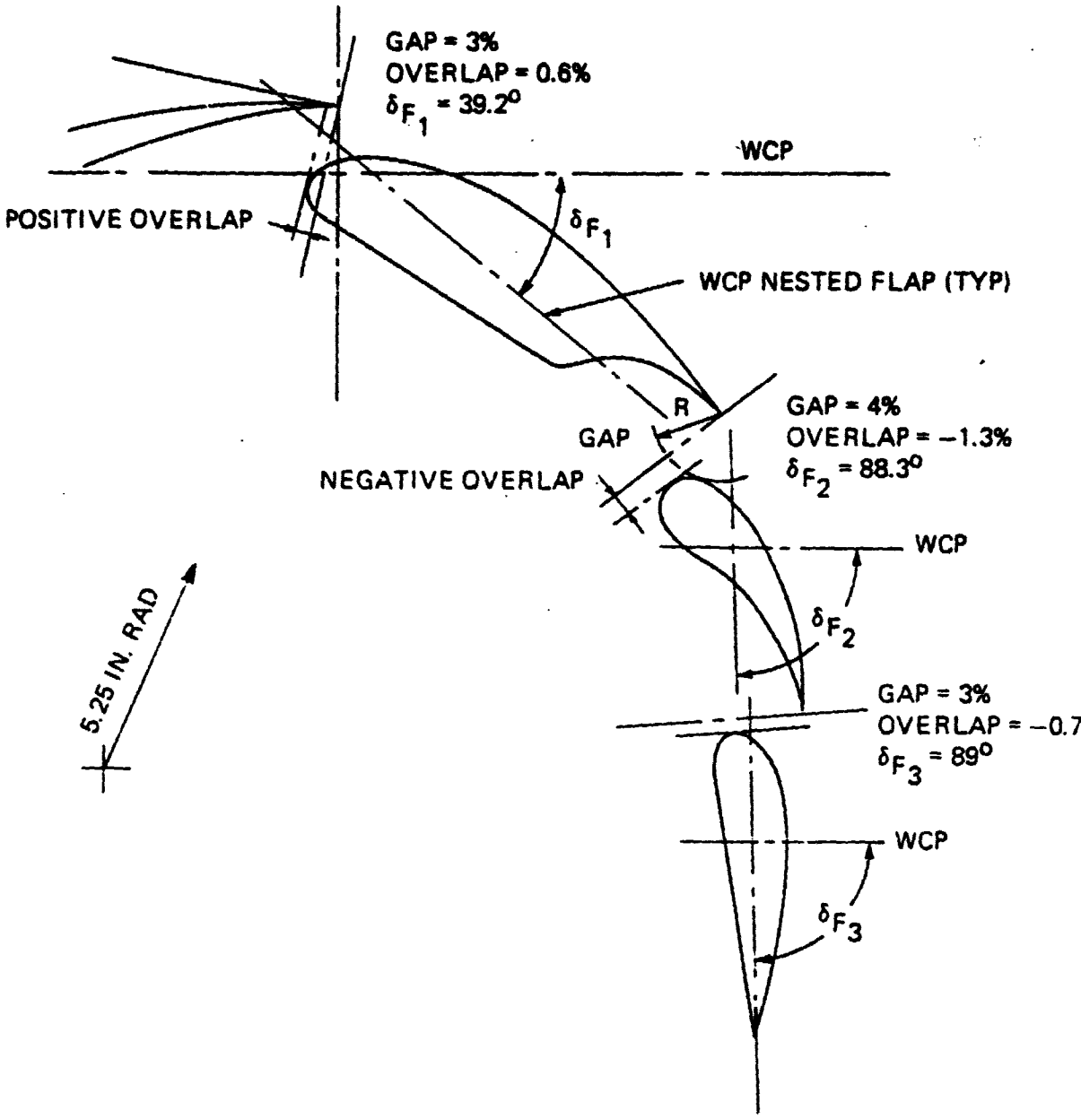

Figure 2–3. Reversed basic flap arrangement: best 'B' configuration, $\delta_F = 90^o$

2.3 Nacelle and Nozzle Geometry

A schematic drawing showing the internal arrangement of the cylindrical nacelle, including the location of the choke plates, screen, and total-pressure rake, is presented in Figure 2-4. This drawing also depicts the geometric relationship between the nacelle and wing section. The air pod centerline lies in the wing-chord plane and is mounted equidistant (spanwise) between the flap tracks.

Prior to this test, a 1/4-inch-thick flow-splitter plate had been added to the model for purposes of other testing which had followed that reported in reference 1. This splitter plate was allowed to remain in place for the current test. As shown in Figure 2-4, the plate extends laterally from the outside of the feedpipe to the inside wall surface of the air pod cylinder. Longitudinally the splitter is butted against the high-pressure choke plate and low-pressure choke plate surfaces and extends rearward past the screen and vertical total-pressure rakes. The trailing edge is blunt, a clean sheared surface. The horizontal total pressure rakes, which were in place for the testing of reference 1, were removed when the splitter plate was installed.

Details of the airflow are shown in Figure 2-5. Compressed air directed up the 0.038 by 0.076-m (1.5 by 3-inch) hollow box section of the wing was introduced into the blown pod via the centerbody feed line (1-3/8-in. id) fastened to the front part of the box section. This air exited from the feed line through four slots 1/2 inch wide and 2 inches long at the forward end of the line and thence into the high-pressure pod plenum via a 90-degree change in flow direction. An additional 90-degree flow change was required to pass the air, in turn, through a high-pressure choke plate with 218 holes, a low-pressure choke plate also with 218 holes, a screen, past an 8-tube vertical total-pressure rake and the end of the splitter plate, and then into the split nozzle. Mass flow into the pod was remotely adjusted from the test-panel-mounted control system. The choke plates and screen are 1.8 inches apart. The screen is stainless steel, with 61.5 percent open area.

Figure 2-6 describes the blown-nacelle nozzle used for this test. This nozzle translates from a cylindrical section at the forward face to a rectangular shape at the exit. The 0.02-square-meter (31.32-square-inch) exit, located at 32 percent of the basic wing chord, was designed to pass one part of the total nozzle mass flow over the top surface of the wing and three parts below the bottom surface. The division of the flow was based on the flow geometries which would achieve optimum thrust recovery and flow turning for the upper- and lower-surface jet flow. The ratio of upper-surface nozzle height to turning radius for optimum turning and thrust recovery was established in previous tests. The largest height of the lower-surface jet was established which would be within the influence of the extended flap system for optimum turning. These conditions showed that a division of 1:3 gave the best operating level for achieving the desired results. This figure also depicts the upper and lower nozzle eyebrows attached to the outer edges of the rectangular exit. Each eyebrow extended over the full breadth of the exit. When this modification was installed, the added nozzle length did not include an extension on the sides of the exit.

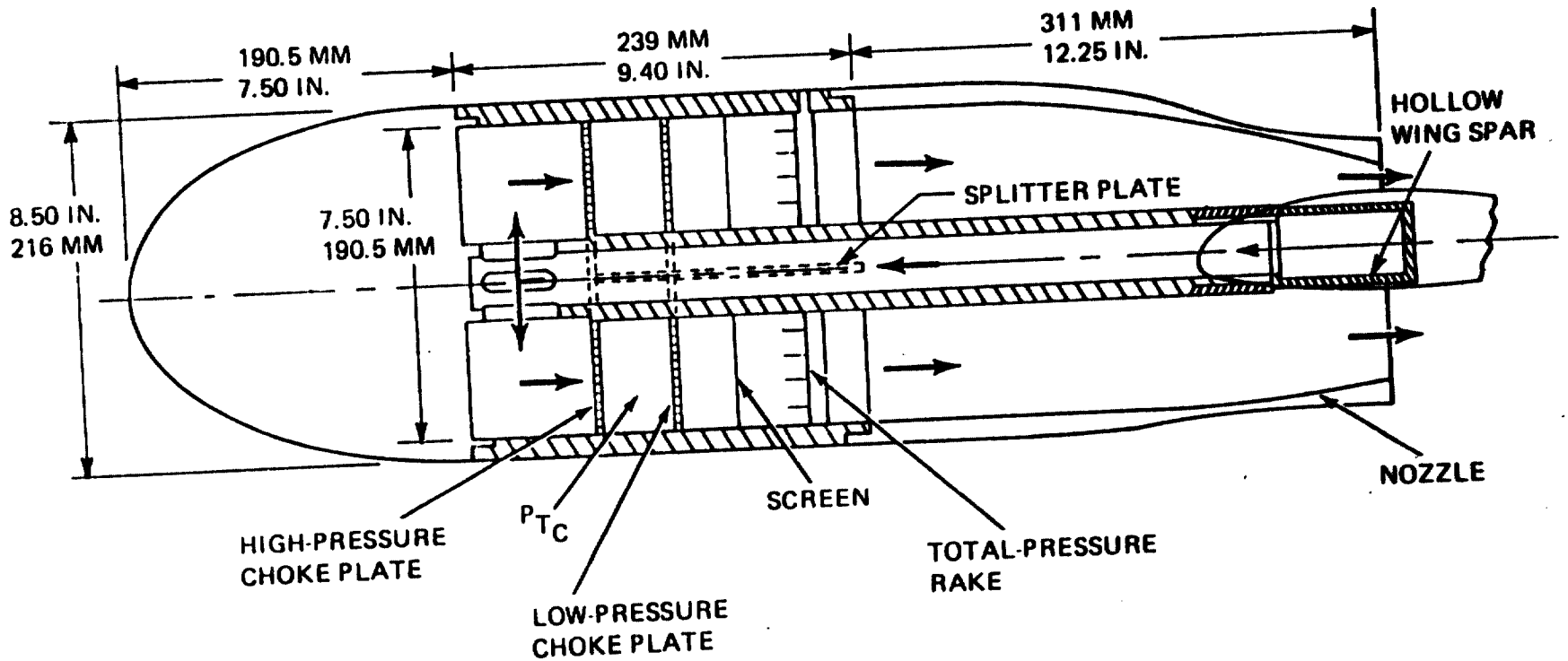

Figure 2–4. Air pod

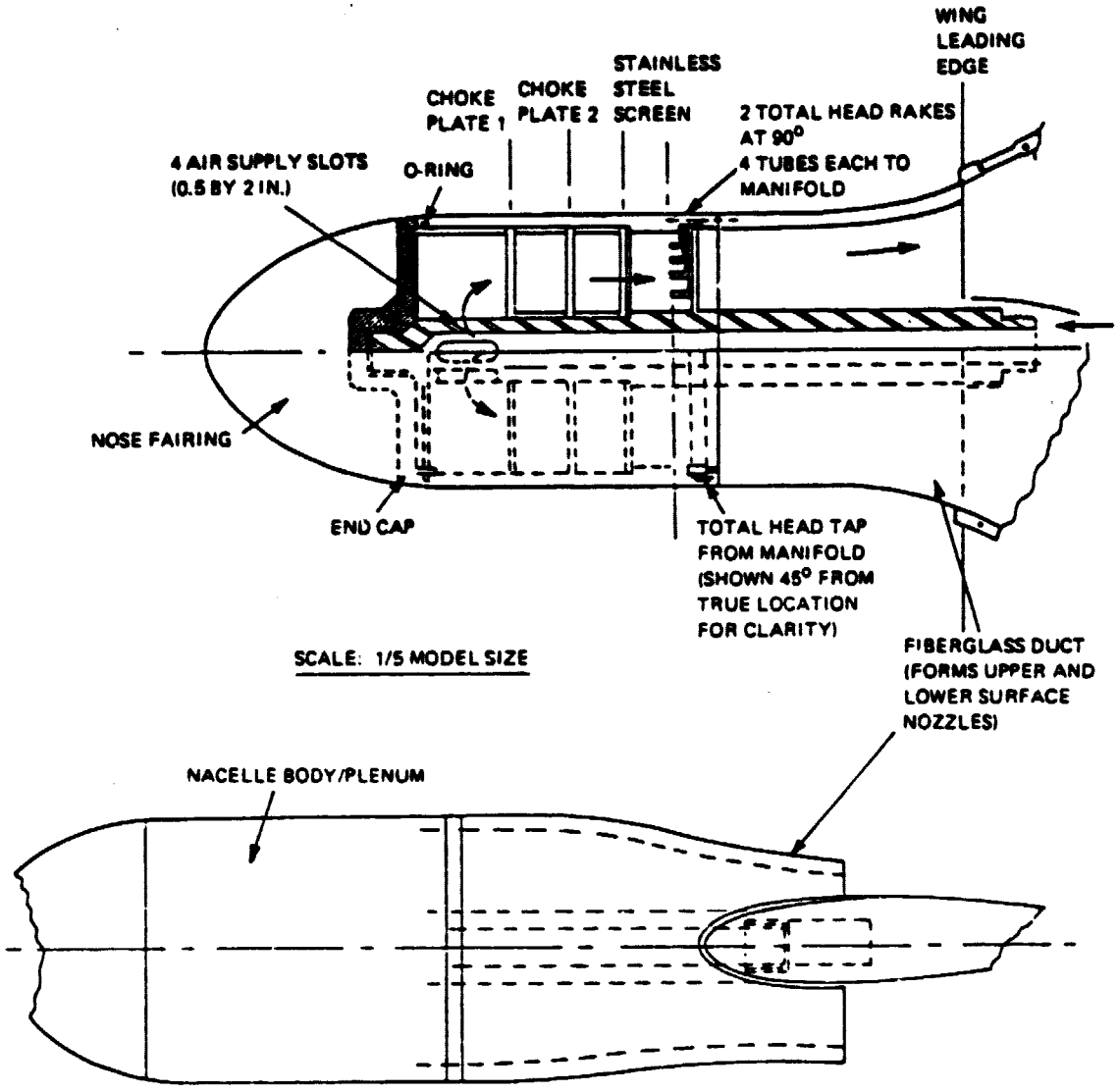

CHOKE PLATES		
R-IN.	NO HOLES	RADIAL SPACING
1.27	28	12° 51' 25"
1.56	34	10° 35' 17"
1.85	40	9°
2.14	46	7° 49' 34"
2.43	53	6° 47' 31"
2.72	59	6° 8' 4"
3.01	65	5° 32' 17"
3.30	72	5°
3.59	78	4° 36' 54"

HOLE DIA NO. 1 – 1/8 IN.

HOLE DIA NO. 2 – 11/64 IN.

SCREEN: 12 MESH, 0.018 IN. DIA, 61.5% POROSITY

Figure 2–5. Details of air pod

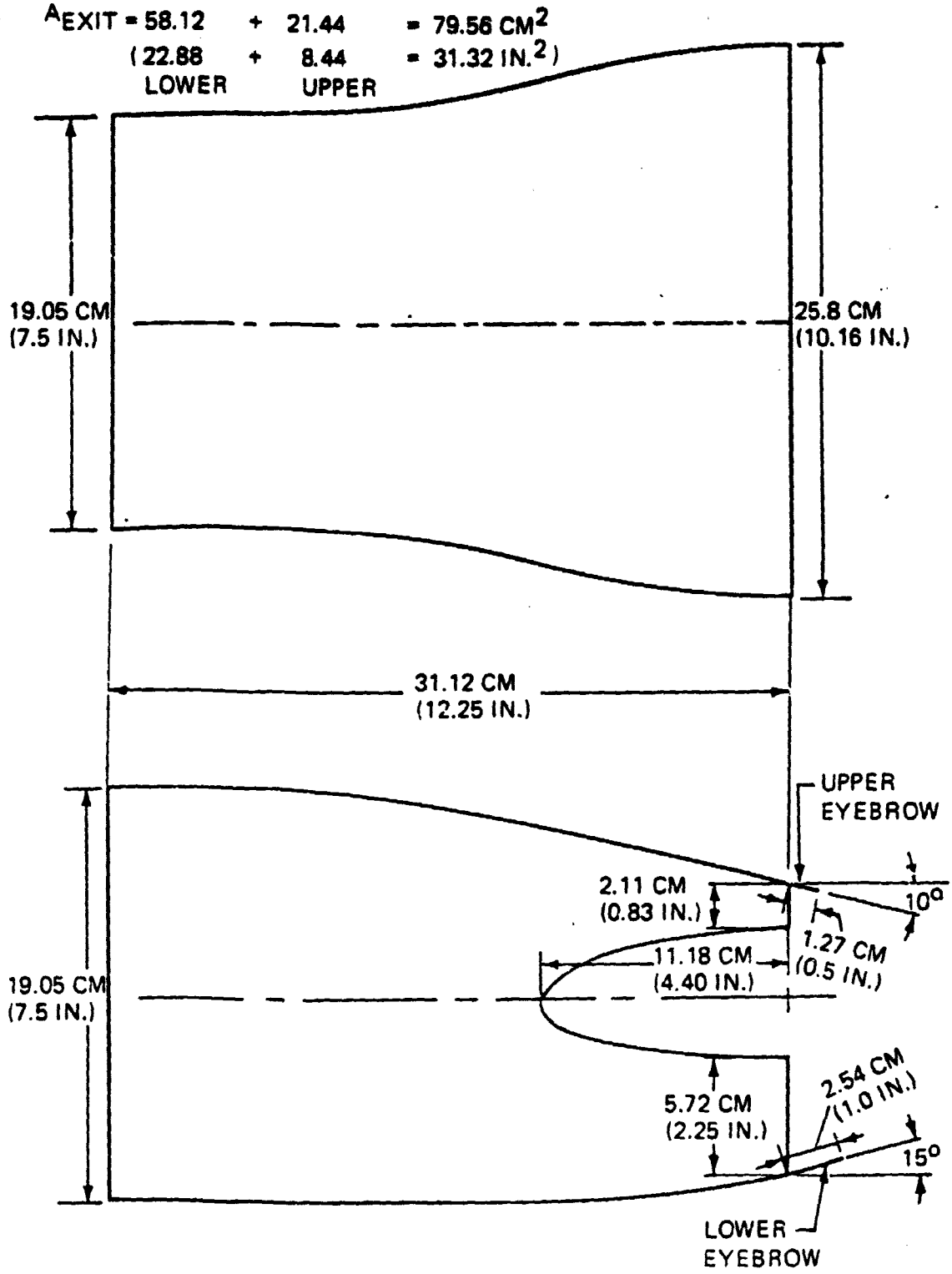

Figure 2–6. Combined surface blowing nozzle

2.4 Probe Traversing Supports

The probe traversing supports and mechanism for the split film and Kiel probes are shown in Figure 2-7. The maximum travel of the hydraulic actuator was 3.5 inches, but this was reduced according to the fittings required at each of the locations and the zero position which was fixed by the relative location of the rig and the surface at that station. The traversing action was done by remote control along a selected axis: along the probe stem axis when traversing perpendicular to the wing, and normal to the stem when traversing chordwise along the slot openings. The spanwise locations were fixed manually along the rods and the rods were moved manually to each location. Two sets of probes, traversing mechanisms, and rods were provided so that measurements could be made near the upper and lower surfaces for each run.

2.5 Model Installation

The test was conducted in the 67-foot-diameter plenum chamber of the 20 by 20-foot Boeing Vertol V/STOL tunnel. For this open-throat configuration, the walls and ceiling of the test section were removed and the model was mounted on the floor of the test section through the fixed ground plane (see Figure 2-8). This ground board is 59 inches above the tunnel floor and serves as the plane of symmetry for semispan testing. The balance was located below the ground board along with the air distribution system.

The four-component balance mounted at the base of the wing structure, below the ground board, was attached to a cylindrical post which supported the model to the tunnel yaw mechanism. All yaw table driving gears plus motor are located below the tunnel floor. High-pressure air to the blown-air pod was routed in two pipes along opposite sides of the post mount, around the balance in large loops, and then into the hollow spar of the wing. The entire assembly between the platform and the tunnel floor was enclosed within a cylindrical fairing that permitted the model to be yawed ±90 degrees in angle of attack. The 17-inch loops (measured from the model axis) of the air pipes around the balance dictated a fairing diameter of approximately 3 feet. Balance calibrations verified that the airpipe routing virtually eliminated any balance interactions due to high-volume air passage. No yawing was performed during this test.

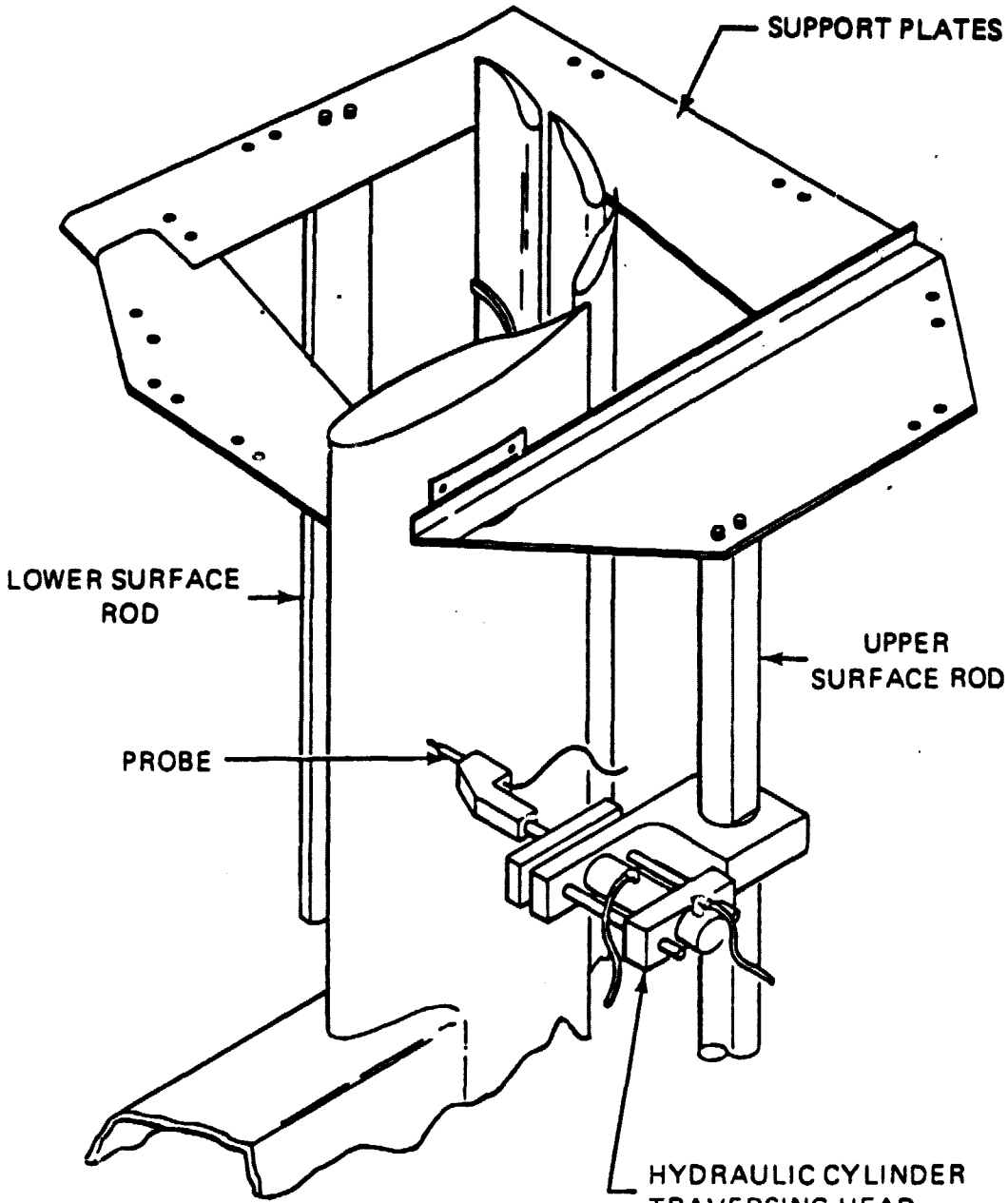

Figure 2–7. Probe traversing supports and mechanism

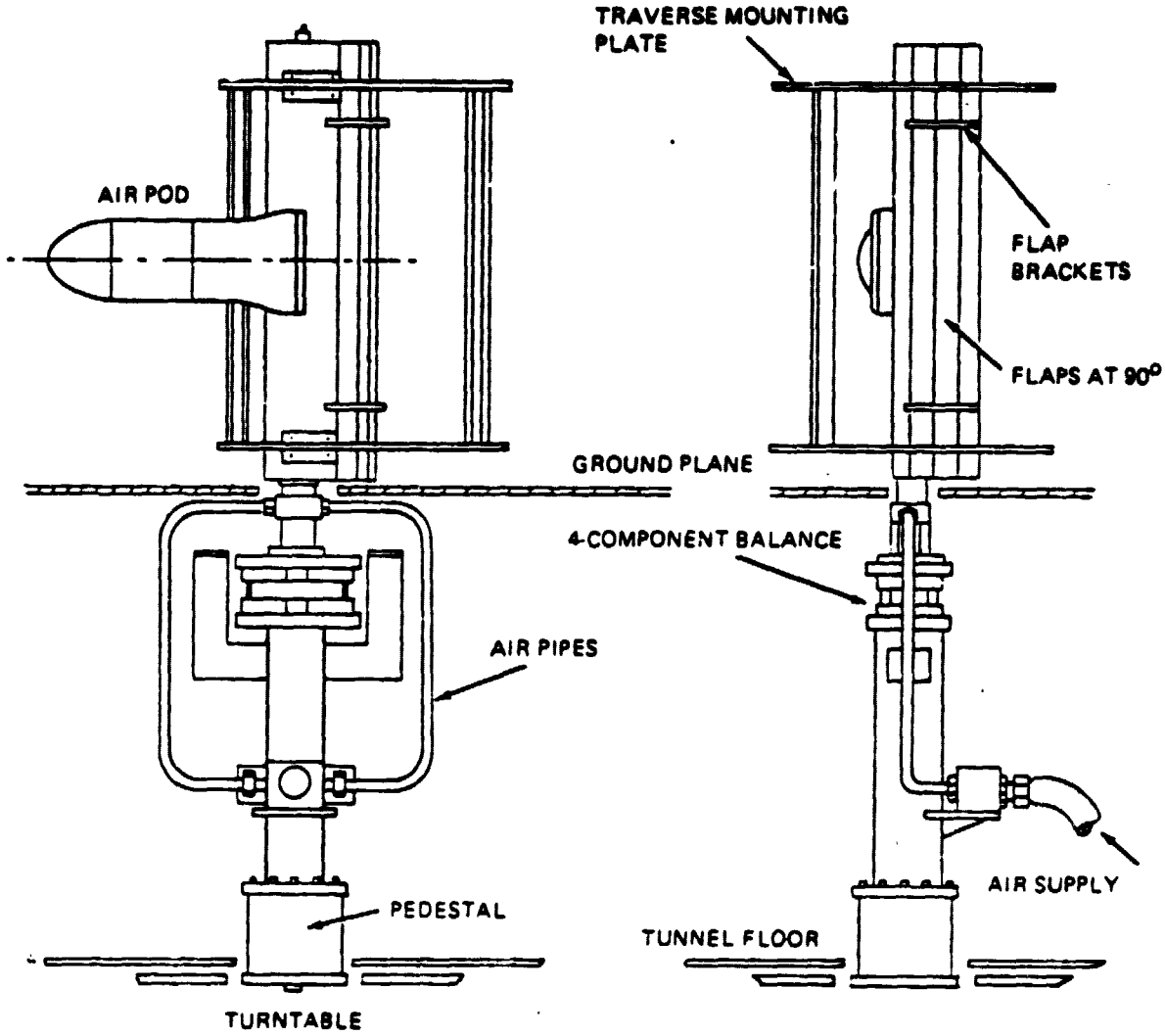

Figure 2–8. Wind tunnel mounting of combined surface blowing model

3.0 INSTRUMENTATION AND EQUIPMENT

3.1 Air Supply and Balance

Air supply. – The wind tunnel auxiliary-air-supply system contains an ASME nozzle for measuring the mass flow through the air pod. Air supply instrumentation included the ASME nozzle temperature, pressure, and differential pressure, and the tunnel static pressure and temperature.

Air-pod total pressure. – The pod total pressure, used to calculate pod pressure ratio and derive other parameters such as thrust recovery, was measured with an 8-tube vertical rake installed in the cylindrical section of the pod just forward of the nozzle. The 8 pressure pickups were averaged by manifolding the pitots into a single outlet tube. The position of the pressure rake is shown in Figure 2-4. The 8-tube horizontal rake used in the test program of reference 1 had been removed prior to this test, to make way for a flow splitter plate.

Air-pod total temperature. – A thermocouple was installed on the air-pod pressure rake to measure the total temperature required for calculating the nozzle coefficients during the calibration runs and the corrected weight flow during the transition testing.

Four-component strain-gage balance. – This balance was inserted between the base of the wing structure below the ground board and the post mount with its axis parallel to the wing-chord line. Thus, yawing the model would turn the balance with the wing. Components measured by the balance were normal force, axial force, pitching moment, and rolling moment.

3.2 Model Instrumentation

This section describes the additional instrumentation provided for the flow survey tests.

From the tests of reference 1, it was speculated that the flow in the wing cove was separated. In order to substantiate this hypothesis, static pressure ports were installed in the cove and on the upper surface of the first flap element along the centerline of the nozzle and at a station 6.13 inches from the centerline. This outboard station is 1.75 inches inboard of the flap bracket. The location of the ports is shown in Figure 3-1. The ports were connected to scanivalves to facilitate data acquisition.

The flow surveys consisted of velocity and total pressure data at specified locations on the flaps as shown in Figure 3-2. A Thermo-Systems Model split film probe was used for the velocity measurement and a miniature Kiel probe was used for the total-pressure data. The split film probe has two sensing elements deposited along the wire which can be used to determine both the velocity and flow angularity with respect to the probe in the plane perpendicular to the probe wire.

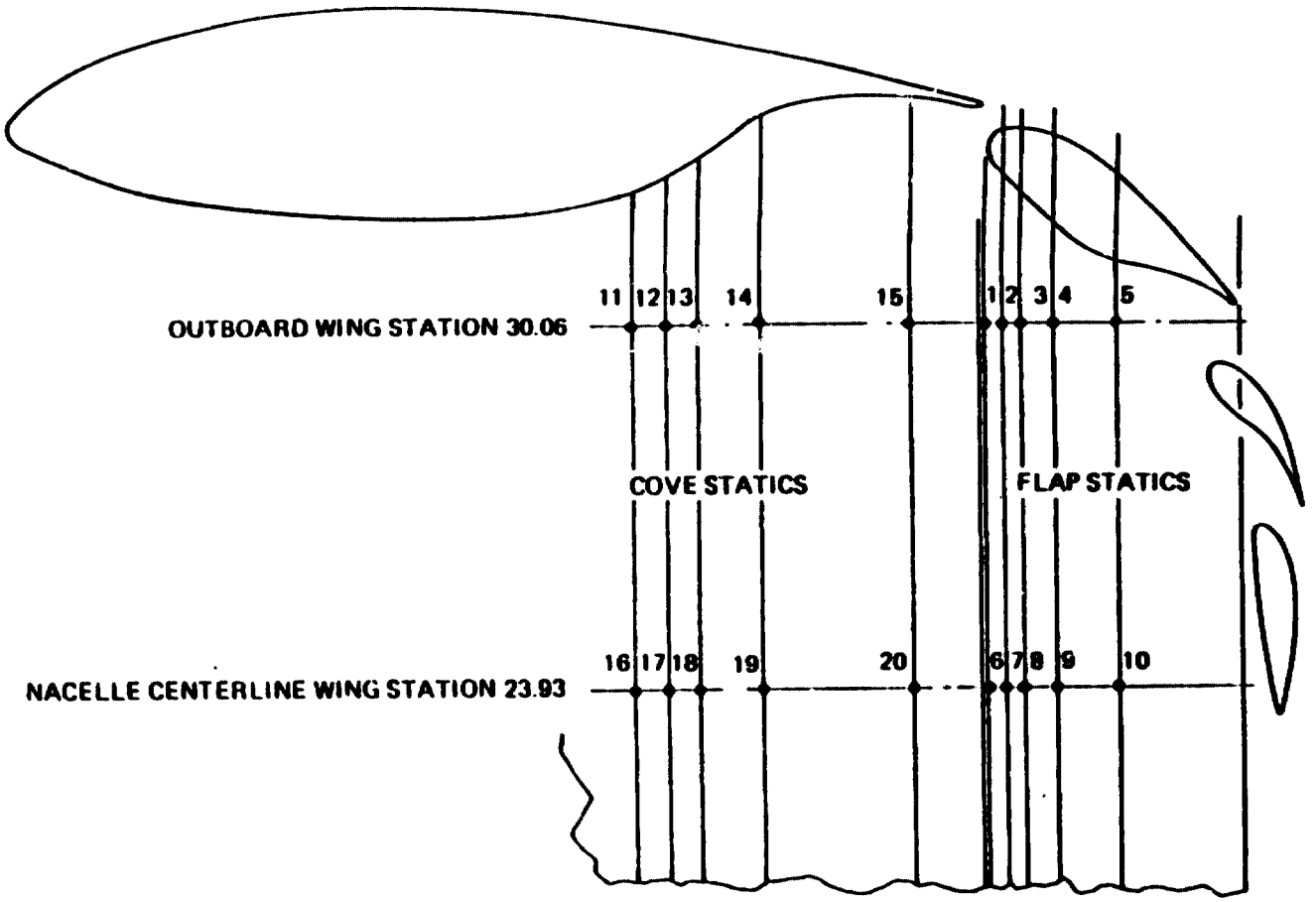

Figure 3-1. Locations of static pressure survey ports

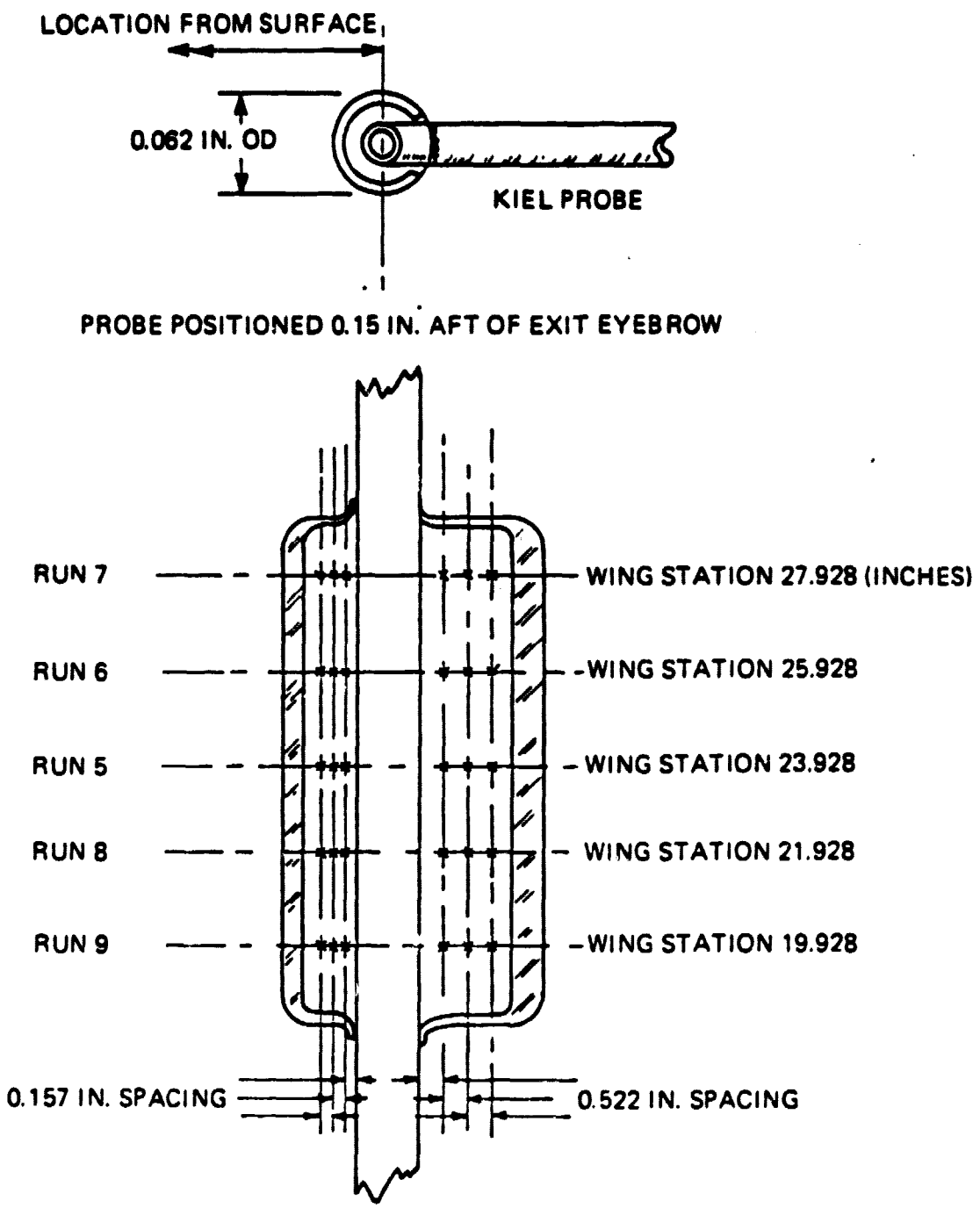

Figure 3–2. Locations of exit survey data acquisition

The instrumentation for measuring the total pressure in the pod was changed from a crucifix with 16 pressure ports to 8 pressure ports consisting of only the vertical legs. The horizontal legs were eliminated in order to install a horizontal splitter plate which extended just downstream of the pressure rake. The upper and lower legs were joined and piped to a single transducer which was designated as the pod total pressure.

3.3 Data Acquisition System

The data acquisition system is the same as was used in the testing reported in reference 1. with additional signal conditioners for the Thermo-Systems split film probes.

The automatic data system can accept up to 120 channels from the model and the tunnel itself. For this test the following data were taken:

Balance Forces and Moments on Wing (balance no. 5209)
- Axial force
- Normal force
- Pitching moment
- Rolling moment

Blowing Pod
- Total pressure
- Total temperature
- Choke differential pressure

Air Supply
- Tunnel static pressure and temperature
- ASME nozzle temperature, pressure, and differential pressure

Probe Surveys
- Hot film flow angle and velocity
- Kiel probes total pressure
- Probe position

These signals are routed to an IBM 1800 computer for processing and on-line data reduction. The computed results are tabulated by a line printer point by point during a run or can be stored for a postrun tabulation. Six selected variables can be plotted on-line by X-Y plotters. Final data is stored on magnetic tape for additional posttest plotting requirements or reprocessing.

A digital display of any nine channels simultaneously is also available during testing for monitoring purposes. Each monitoring channel can display predetermined prime quantities in engineering units or coefficients that are calculated by separate software and continuously updated during each run. The parameter displayed in each channel can be switched through a control box to a variable more appropriate for a particular run. As a result of the continuous update, a model is usually flown with the aid of a monitoring channel, for example, the calculated ASME air-pod mass flow during the static-performance testing.

4.0 DATA REDUCTION

The test data was reduced on line and presented in both graphic and tabular format to aid in monitoring and conducting the test. Force and moment data were reduced on the IBM 1800 computer.

4.1 Calibration

Thrust calibration runs were made with flaps retracted at the beginning and end of the test period over a range of nozzle pressure ratios from 1.05 to 1.3. Thrust and pressure data from these calibration tests are closely described by a straight line. Curve fit of the data using linear regression analysis shows the coefficient of determination r^2 equal to 0.9989.

4.2 Flow Survey Test Under Static Conditions

During the flow survey tests the primary parameter used was the nozzle pressure ratio, PTN/PL. The rationale for using this as the primary parameter was to fix the flow Mach number.

5.0 TEST PROCEDURE AND TEST CONDITIONS

5.1 Nozzle Survey

A total pressure survey at the exit of the nozzle was made using the miniature Kiel probe for the purpose of comparison with the total pressure survey obtained in reference 1. The survey was conducted at a pressure ratio of 1.25. This survey covered the upper nozzle exit at three vertical locations: the lower nozzle was sampled at three vertical locations also. The total pressure profile, Figure 5-1, shows approximately 2-percent scatter for all vertical locations in both nozzles except at the inboard edge. The scatter of reference 1 is shown for comparison. Differences at the edges may be attributable to the influence of the splitter plate which was installed in the pod as discussed in paragraph 2.3.

5.2 Wing Cove Pressure Survey

Possible flow separation in the wing cove was explored by measuring the pressures at fixed pressure port locations in the cove and the upper surface of the first flap element (Figure 5-2). The tests were conducted at pressure ratios of 1.2 and 1.3 to determine if compressibility effects could be detected in the region from Mach 0.5 to 0.6. No flow measurements were taken during this test.

5.3 Velocity Profile Survey

The split film data for the velocity profiles were taken at the predetermined control stations shown in Figure 5-3 at a pressure ratio of 1.2. The centerline of the nozzle (wing station 24.05) was a survey station and two lateral positions were surveyed at the beginning of the tests, at wing stations 30.93 and 29.93. The flap bracket is located at wing station 31.93 inches and therefore the two locations were 1 inch and 2 inches inboard of the flap bracket or 1.8 and 0.8 inches outboard of the nozzle. The outboard survey station was originally set within 1 inch of the flap bracket so as to be within the central jet flow and away from the bracket. However, the velocities were so small at this location that the probe was reset 2 inches inboard of the flap bracket. The chordwise locations were set at the entrances and exits of the slots, near the leading and trailing edges of the flap elements, and at the maximum-thickness chord positions of the upper surface. The on-line velocity data showed that the velocities at both outer stations were small. The velocities at wing station 29.93 inches were slightly higher (about 15 percent, or 20 to 50 fps) than at wing station 30.93 at the first chordwise survey stations on the upper and lower surfaces, stations 1 and 17, Figure 5-3. The velocity data at these two lateral stations were taken in order to show the amount of spreading of the nozzle flow and/or entrainment of flow into the efflux.

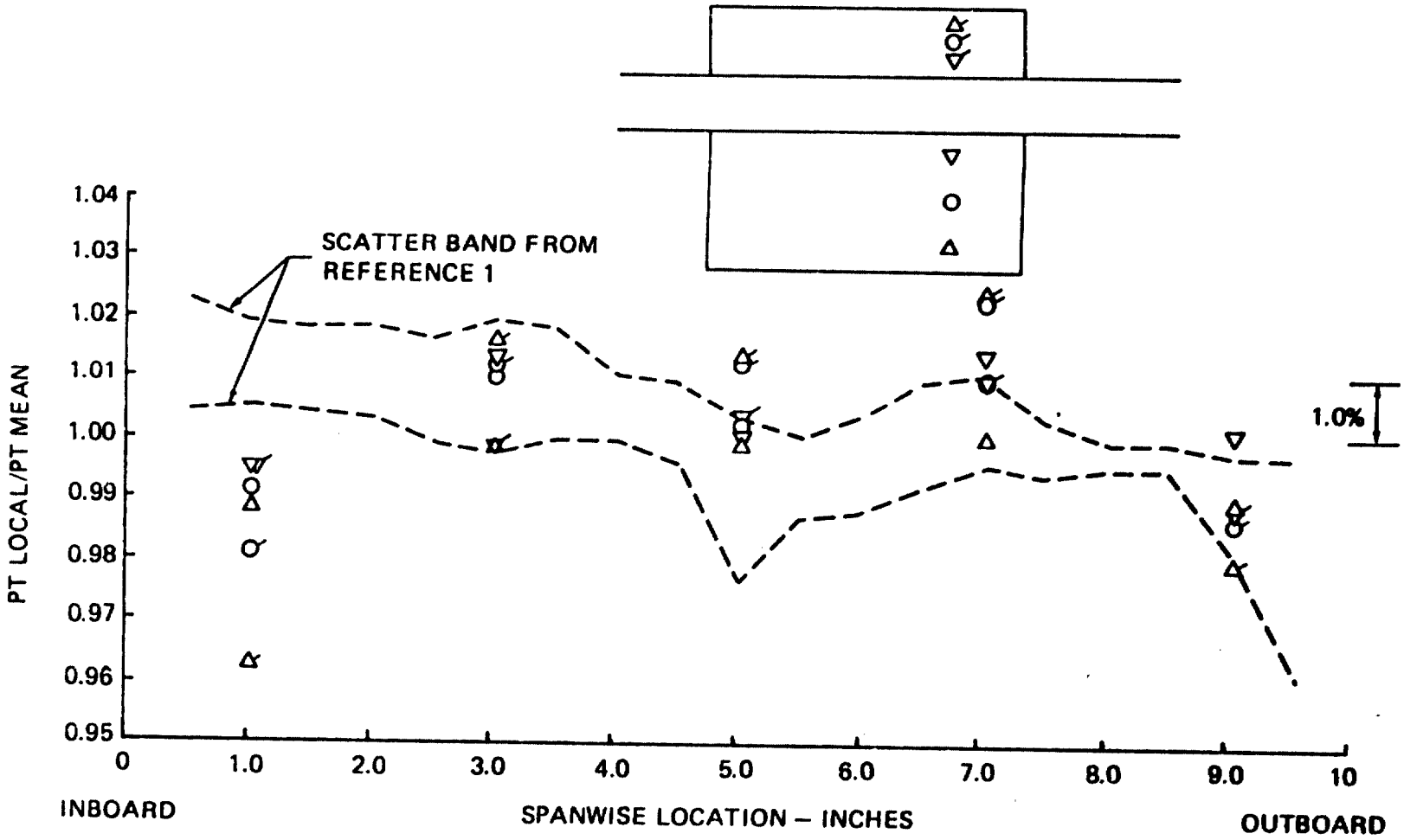

Figure 5–1. Total pressure survey at nozzle exit

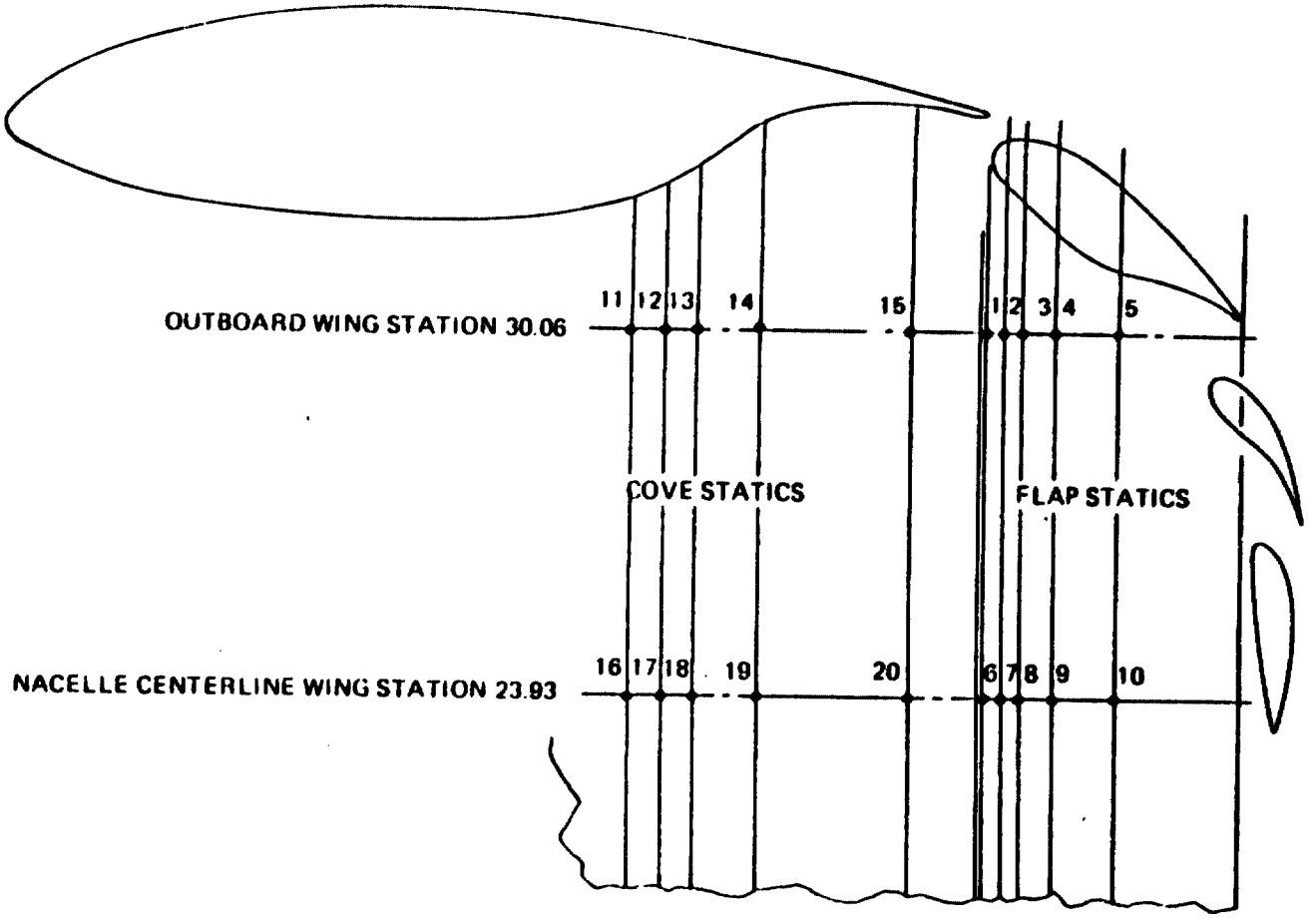

Figure 5–2. Location of cove pressure taps

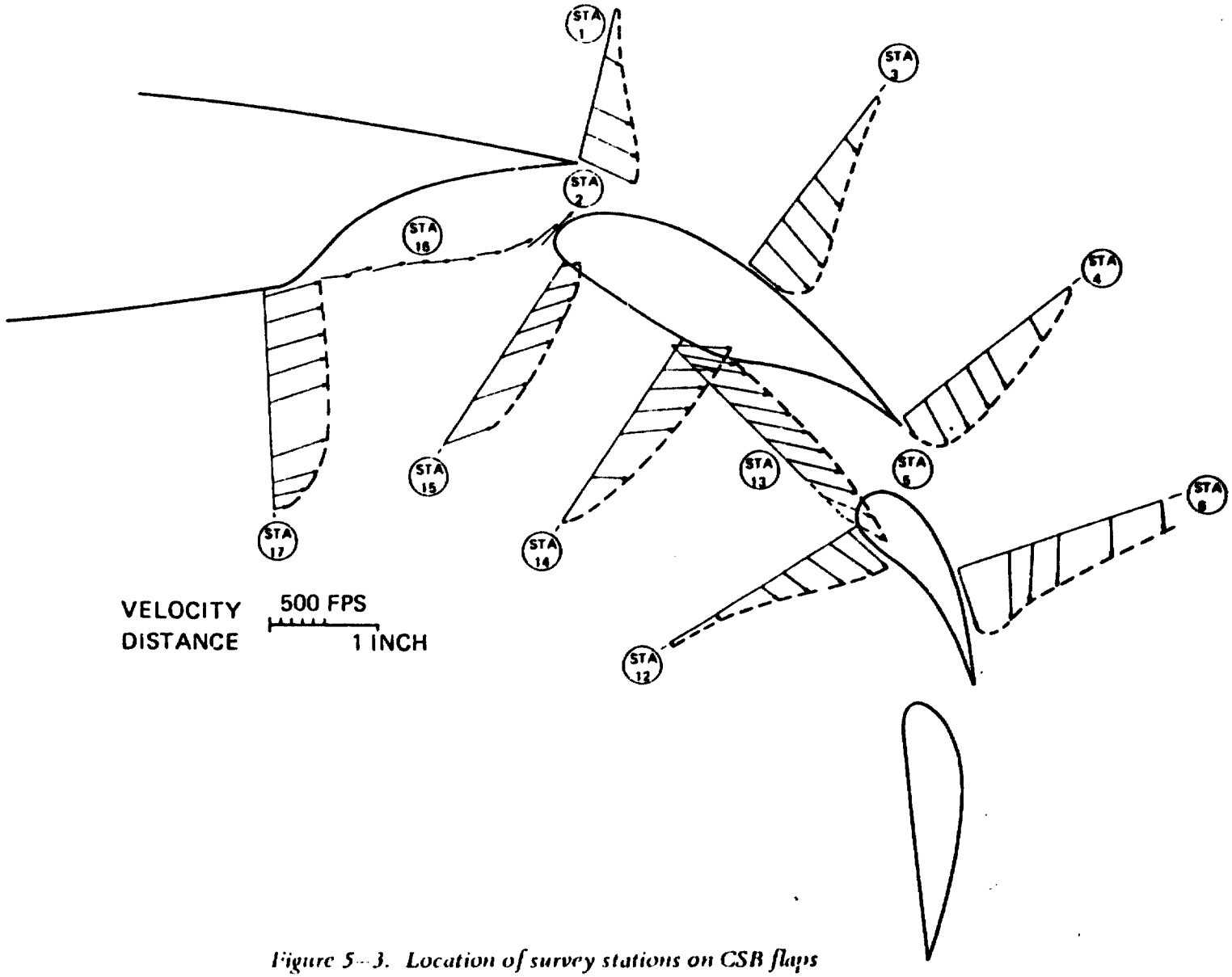

Figure 5--3. Location of survey stations on CSB flaps

Remote positioning of the probe away from the surface was done from the wind tunnel control room by monitoring the visual display from the position transducer. The reference positions of the probes were established prior to each run. The chordwise locations were established prior to each run. The chordwise locations were established by resetting the upper and lower surface rods to the appropriate locations on the mounting plates. The hydraulic cylinder traversing heads were manually located at each of the two spanwise positions on the rods.

In order to evaluate the spanwise flow an attempt was made to measure the lateral velocity using the split film probe. However, the probe was destroyed by the large dynamic pressure of the chordwise flow impinging laterally on the probe when positioned in this manner.

The thrust recovery calculated from the balance data at the nozzle pressure ratio of 1.2 was 0.88, compared to the thrust recovery of 0.89 reported in reference 1.

5.4 Total Pressure Survey

The total pressures were measured at the positions corresponding to the split film surveys using the same probe holders, traversing mechanism, and brackets. The reference positions of the probes were established at the start of each run and the operating procedures for the survey were the same as those used for the split film survey. Although the pressure data were displayed plotted on line, they did not include the corrections for the flow angularities.

5.5 Turning Effectiveness

The performance parameters for the CSB system in terms of the thrust recovery and thrust deflection angle for this test were comparable to the data of reference 1. The thrust recovery factor is defined as the ratio of the resultant force to the reference thrust:

$$\text{Thrust recovery} = \frac{\text{Resultant force}}{\text{Reference thrust}}.$$

The reference thrust is the thrust available from the blowing pod at that pressure ratio when operating as a pure jet.

The thrust deflection angle is the angle defined by the normal force and axial force when the CSB system is operating with the flaps deployed:

$$\text{Thrust deflection angle} = \tan^{-1}\left(\frac{\text{Normal force}}{\text{Axial force}}\right).$$

The nominal values for this test and for the static test of reference 1 are:

	This Test	Reference 1
Thrust recovery	0.88	0.89
Thrust deflection angle	86.3 degrees	86.7 degrees

Thus, the operating conditions for the two static tests can be considered equivalent.

6.0 TEST RESULTS AND DISCUSSION

The data in this section cover the flow survey portion of the test. The calibration runs and the probable effect of the splitter plate and total pressure rake changes on the thrust calibration were discussed in previous sections. The data are covered in the following sequence: (1) cove, (2) velocity, and (3) total pressure.

6.1 Cove Pressure Survey

The pressure ports installed in the wing cove were located from the knee entering the cove to the minimum thickness position at the trailing edge of the cove (Figure 6-1). The five pressure ports were located by halving the distance between successive locations going forward from the cove trailing edge, so that the orifices were concentrated toward the entrance to the cove. The five ports in the first flap element were located with a similar doubling of the spacing, starting at the leading edge of the flap and ending at the chord location just aft of the crest.

The pressure distributions shown in Figures 6-1 and 6-2 are for the two nozzle pressure ratios (PTN/PL) of 1.2 and 1.3 and show positive pressures in the flap cove. The pressure rise occurs at a more forward location at the higher pressure ratio. Because of the finite number of pressure ports, the exact point at which the pressure rise occurs cannot be determined. The pressure distributions are indicative of separation along the surface of the cove. Increasing the pressure ratio increases the unfavorable pressure gradient. Further evidence of the separation is given by the velocity profile across the entrance to the first slot. As discussed in paragraph 6.2, the flow is unable to turn the corner at the knee and continues parallel to the entrance until it approaches the leading edge of the flap.

The pressure distribution on the flap shows some interesting deviations from the measurements over a single-slotted flap, shown in Figure 6-3 from reference 2. The flap from that reference is assumed to have local flow that is well-behaved (unseparated), and the pressure distribution is typical for such flaps. The maximum suction pressure on the flap occurs at the exit area from the cove, opposite the trailing edge of the cove. The stagnation point is under the nose of the flap and a rapid acceleration of the flow around the leading edge is obvious. This may result in another suction peak just aft of the stagnation point and forward of the suction peak associated with the cove trailing edge. Furthermore, the pressure at the maximum thickness is neither a maximum nor a minimum.

The data from this test (Figures 6-1 and 6-2) differ markedly from the flapped wing of reference 2. At the pressure ratio of 1.2 a suction peak is located on the flap in the vicinity of the cove exit, i.e., a flow nozzle as with the referenced flap. However, there is an increase in the pressure (minimum in terms of suction pressure) at the third pressure port and a subsequent suction peak in the vicinity of the fourth port at maximum thickness. Neither the stagnation point nor the suction around the leading edge is observable from the pressure data.

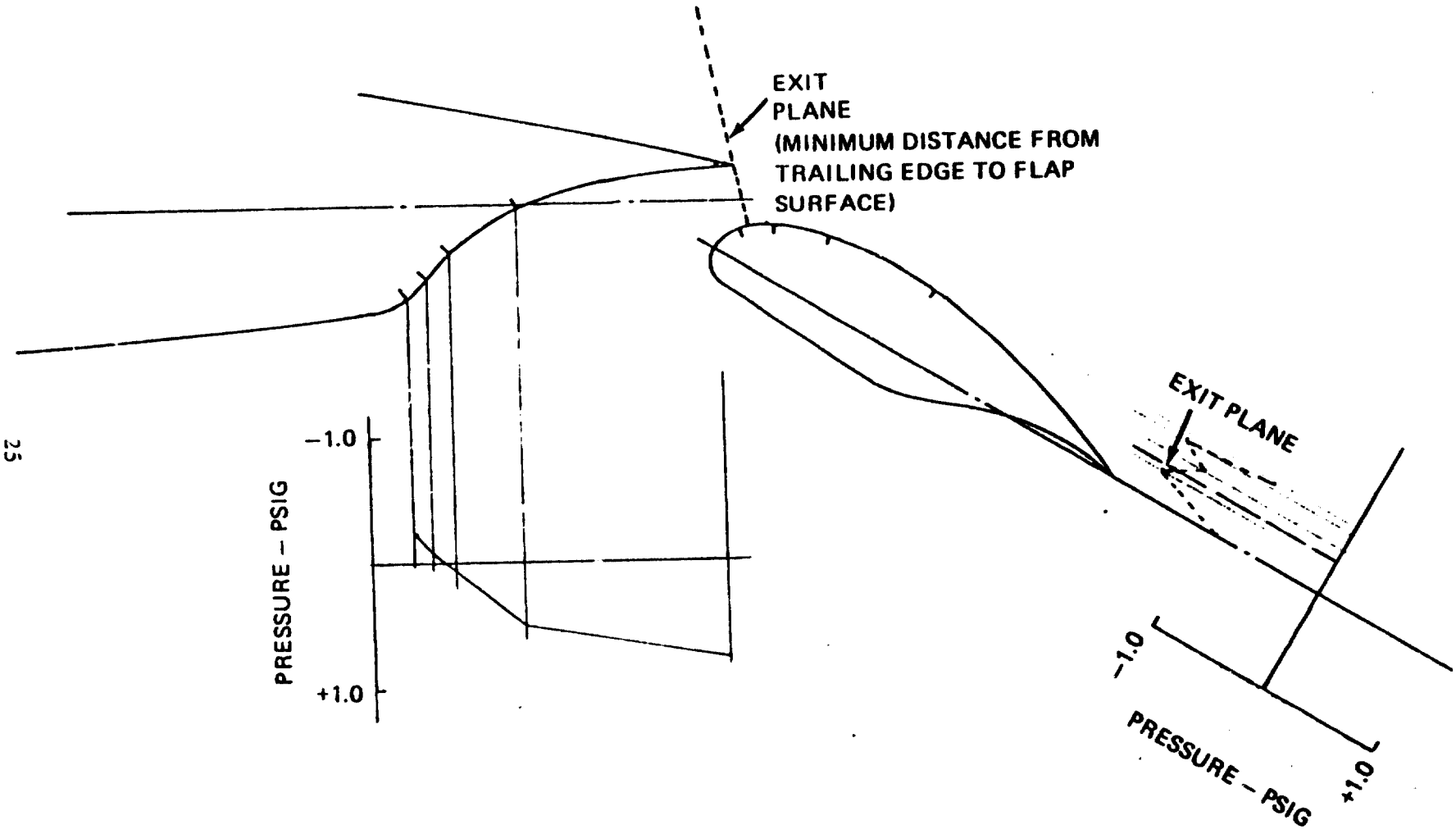

Figure 6–1. Pressures in wing cove along the centerline of nozzle, PT nozzle/PT local = 1.2

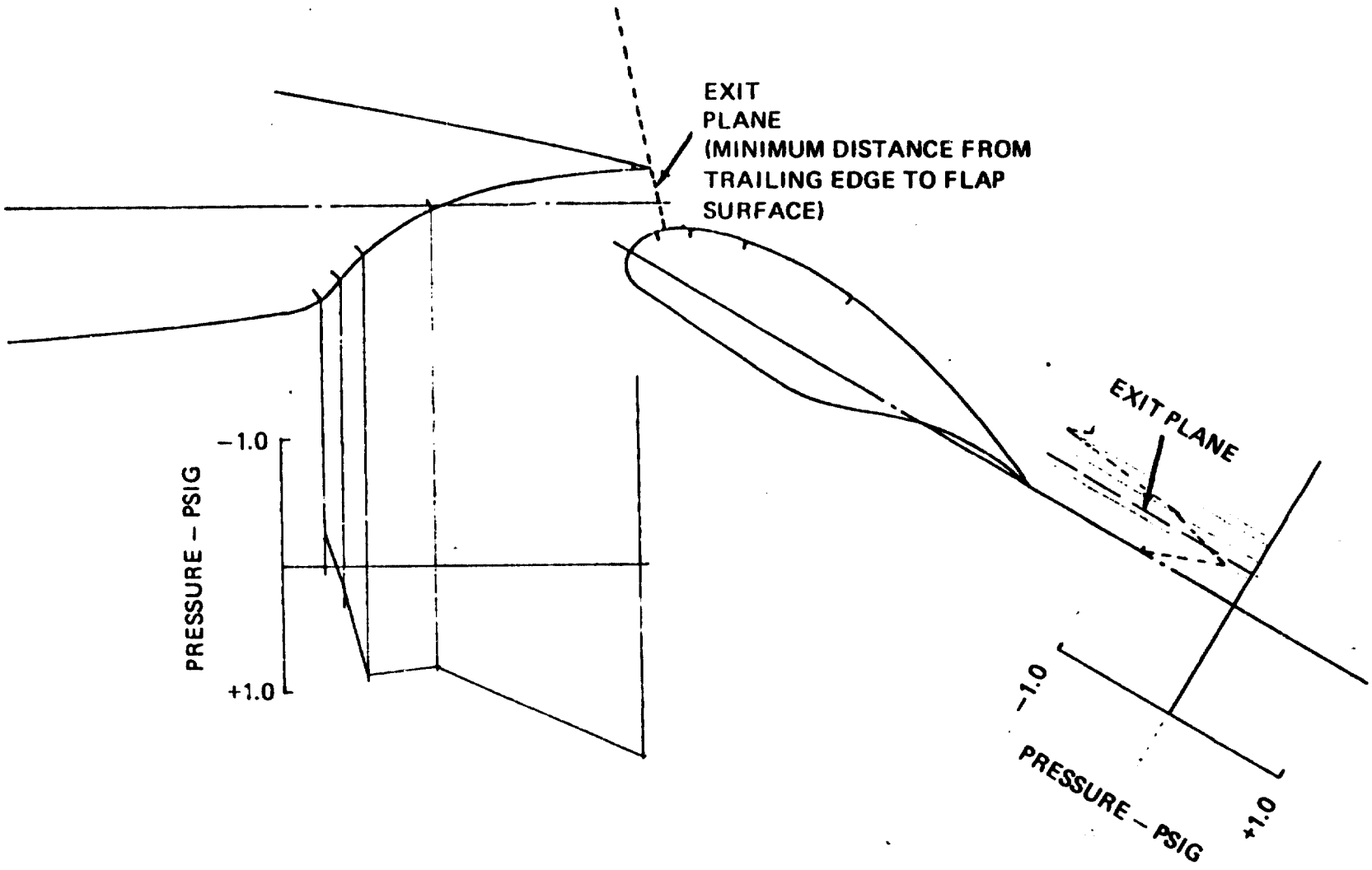

Figure 6–2. Pressures in wing cove along the centerline of nozzle, PT nozzle/PT local = 1.3

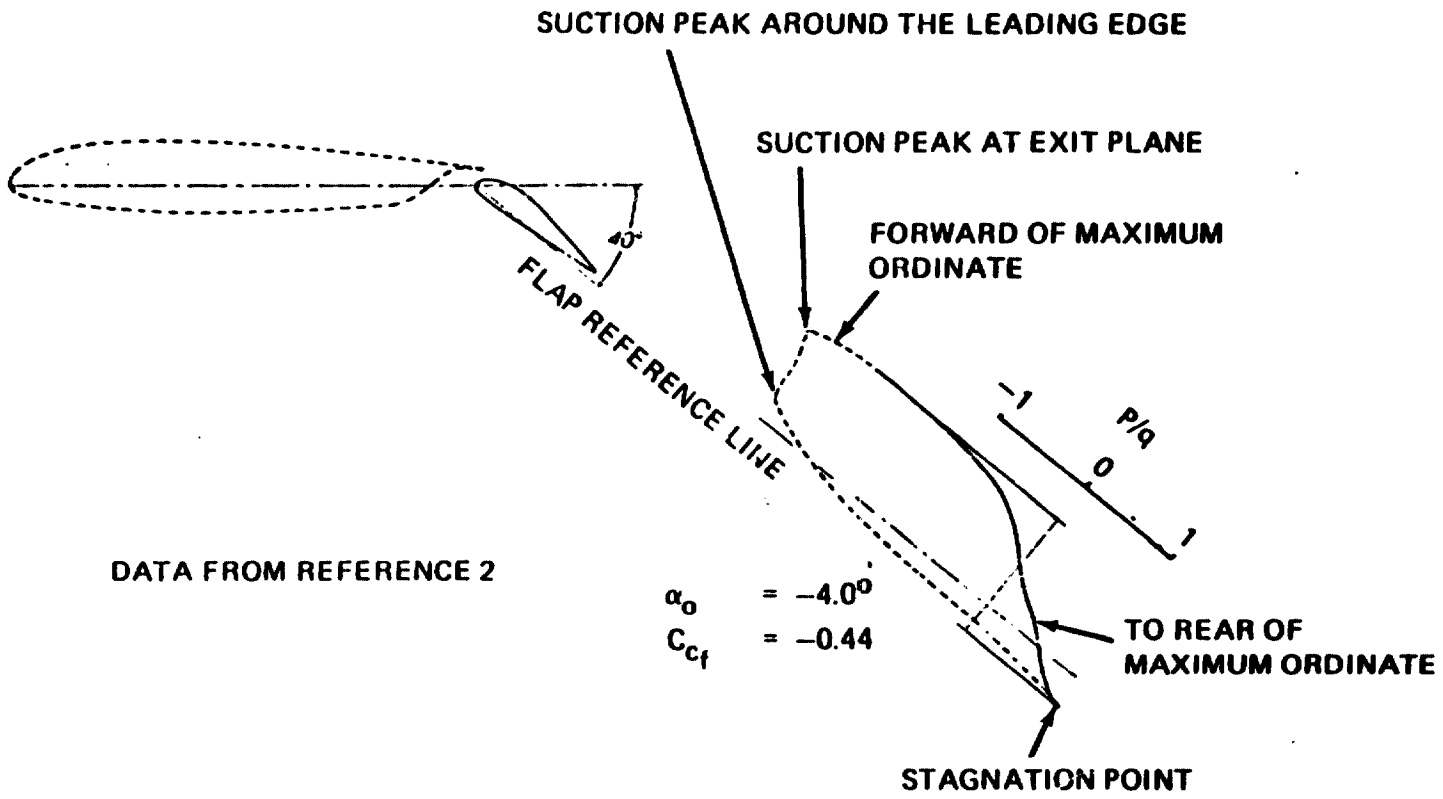

Figure 6--3. Chord pressure distribution on a 0.2566-chord slotted flap mounted on the NACA 23012 airfoil

When the pod pressure ratio ir increased to 1.3, large changes occur. The suction peak in the vicinity of the maximum thickness increases, but the suction pressure expected from venturi effect at the cove exit plane disappears. At 1.3 pressure ratio, the suction pressure increases toward the leading edge of the flap with a peak near the leading edge. The flow in the cove is assumed to be separated and seems to have significantly altered the effective flow geometry and the cove exit region is not the minimum area, i.e., venturi of the flap gap nozzle.

6.2 Velocity Survey

The velocity data is presented pictorially in two ways. In Figures 6-4 and 6-5, the velocity profiles show the total velocities and the angularities along the nozzle centerline (wing station 24.05) and along wing station 29.93 inches. This format gives an overview of the flow, particularly as to such features as the inability of the flow to turn into the cove, the large flow into the second slot, and the flow in toward the lower surface of the first flap.

The second format, shown in Figures 6-6 and 6-7, shows the velocities normal to the traversing axis and is a better presentation of the mass flow rate per unit span at each of these stations.

6.2.1 Flow on the upper surface at the trailing edge of the wing cove. – Figures 6-8 and 6-9 are the velocity profiles along the centerline of the nozzle and outboard of the nozzle at wing station 29.93 inches. This location is approximately 6 inches downstream of the upper nozzle. The velocity profile shows that the flow has expanded upward into the ambient air. This expansion also occurs outward laterally as shown in Figure 6-9. The velocity at the outboard station is nearly two-thirds of the centerline velocity and appears to be greatest near the wing surface.

Because of the convex curvature of the upper surface, this flow should be inward toward the centerline of the nozzle. Thus, the increase in velocities at the outboard station going from the nozzle exit down the flap must be the result of the flow spreading due to impingement on the wing or induced flow rather than an expansion of the nozzle flow.

6.2.2 Flow on the lower surface upstream of the wing cove. – This location is approximately 3 inches downstream of the nozzle exit. At the centerline of the nozzle (Figure 6-10), the velocities are nearly constant except away from the surface. The decrease in velocity at that point suggests that mixing with the ambient air begins in that region. The chordwise velocities measured at the outboard station (Figure 6-11) are not large, i.e., 50 to 60 fps, as compared to the nozzle flow velocity, about 300 fps. Although the height of the lower nozzle is approximately three times the height of the upper nozzle, the increased depth of the mixing region, the lower surface appears to have a smaller chordwise induced flow at the outboard station compared to the upper surface flow.

6.2.3 Wing cove inlet flow. – The velocity profile shown in Figures 6-12 and 6-13 shows that the centerline flow and the outboard flow cannot negotiate the turn into the cove. For

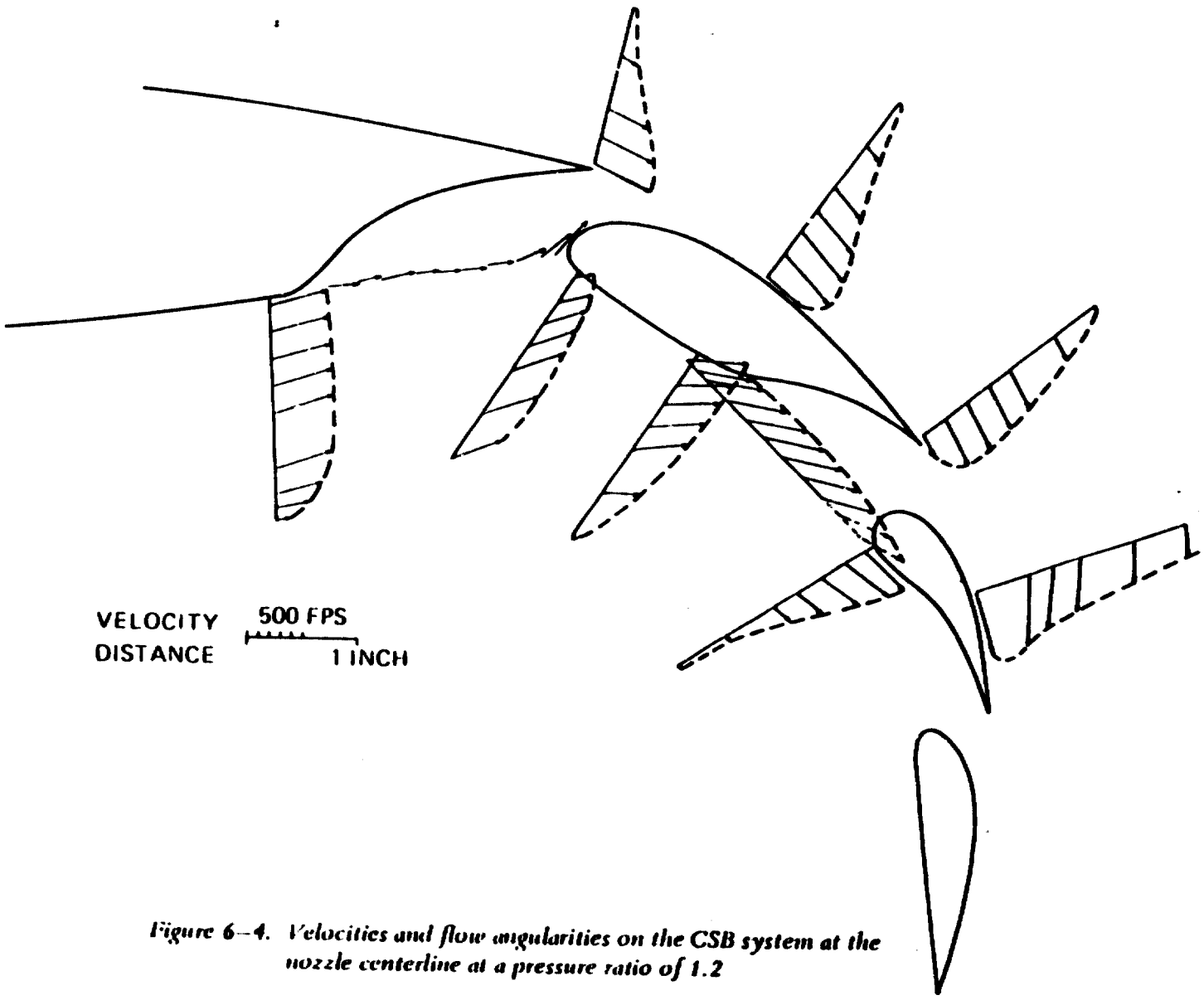

Figure 6–4. Velocities and flow angularities on the CSB system at the nozzle centerline at a pressure ratio of 1.2

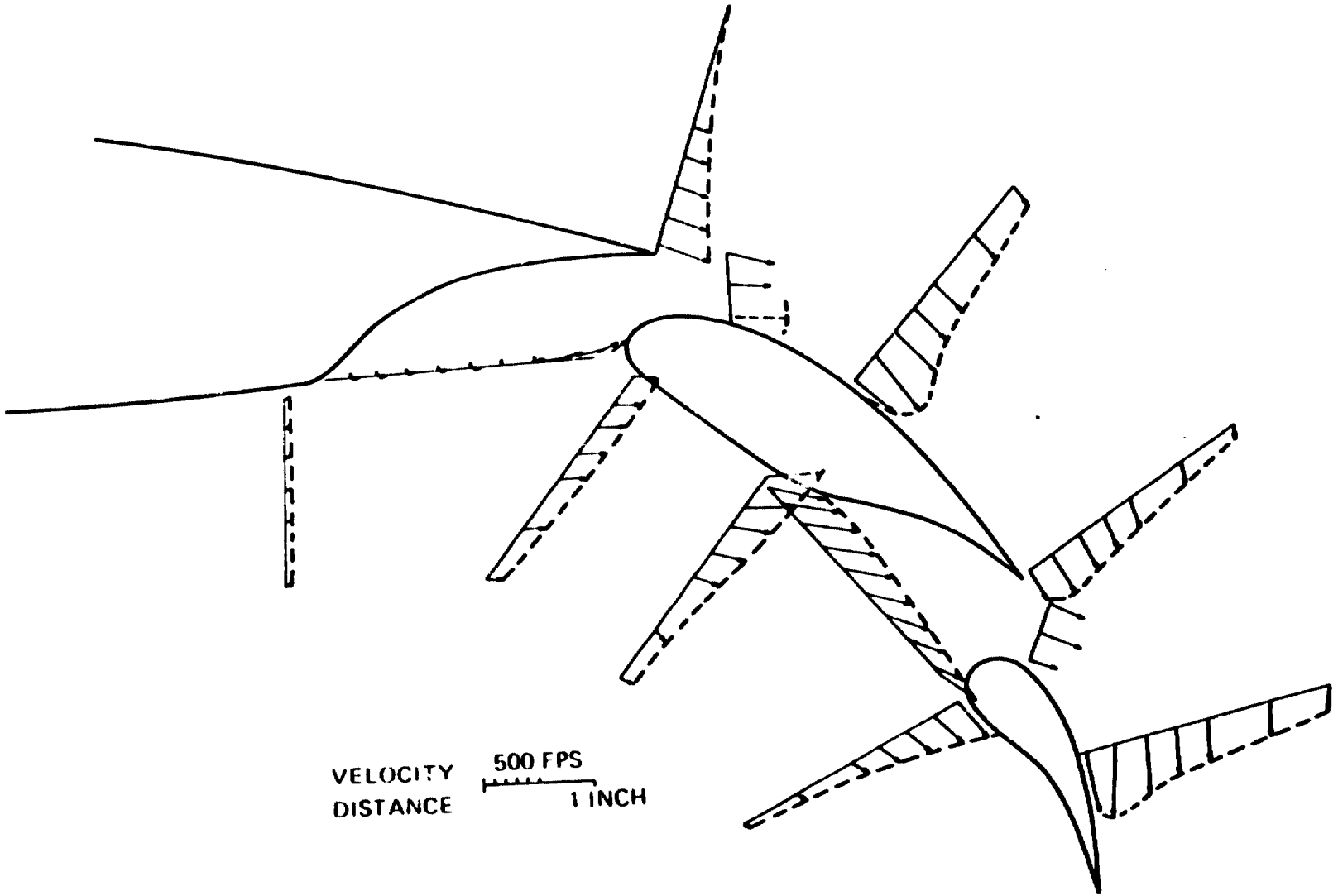

Figure 6-5. Velocities and flow angularities on the CSB system at wing station 29.93 inches at a pressure ratio of 1.2

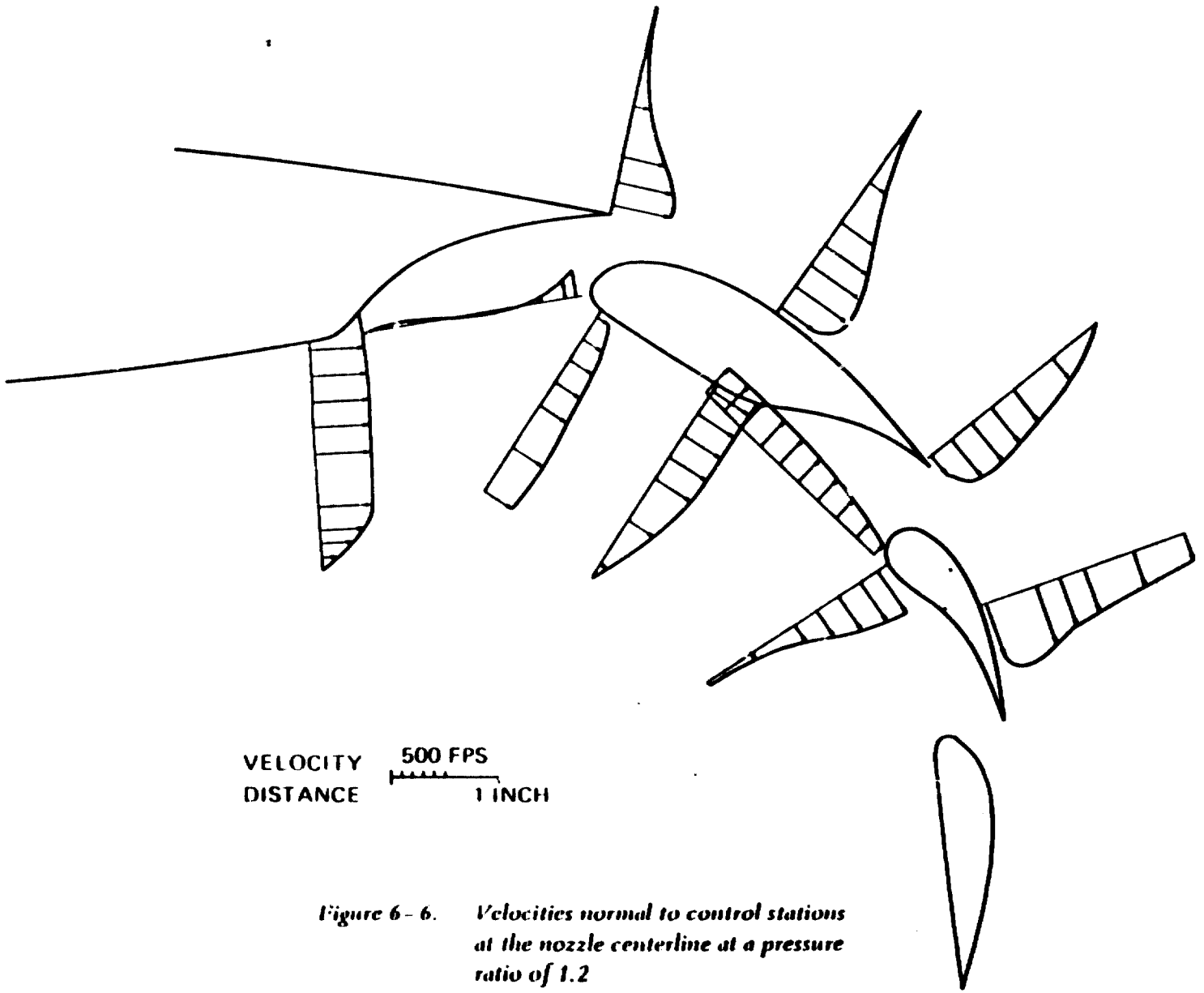

Figure 6 - 6. Velocities normal to control stations at the nozzle centerline at a pressure ratio of 1.2

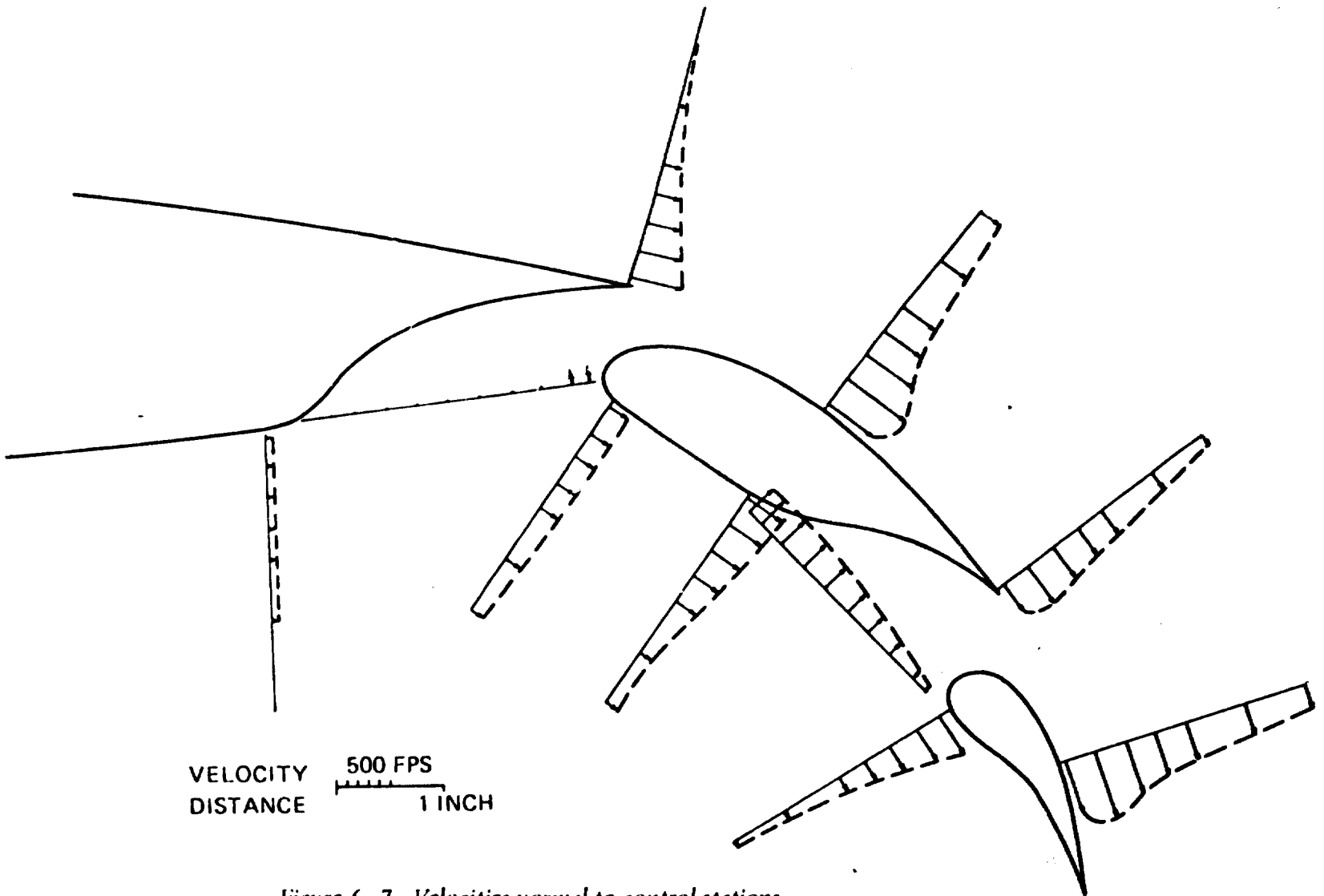

Figure 6–7. Velocities normal to control stations at wing station 29.93 inches at a pressure ratio of 1.2

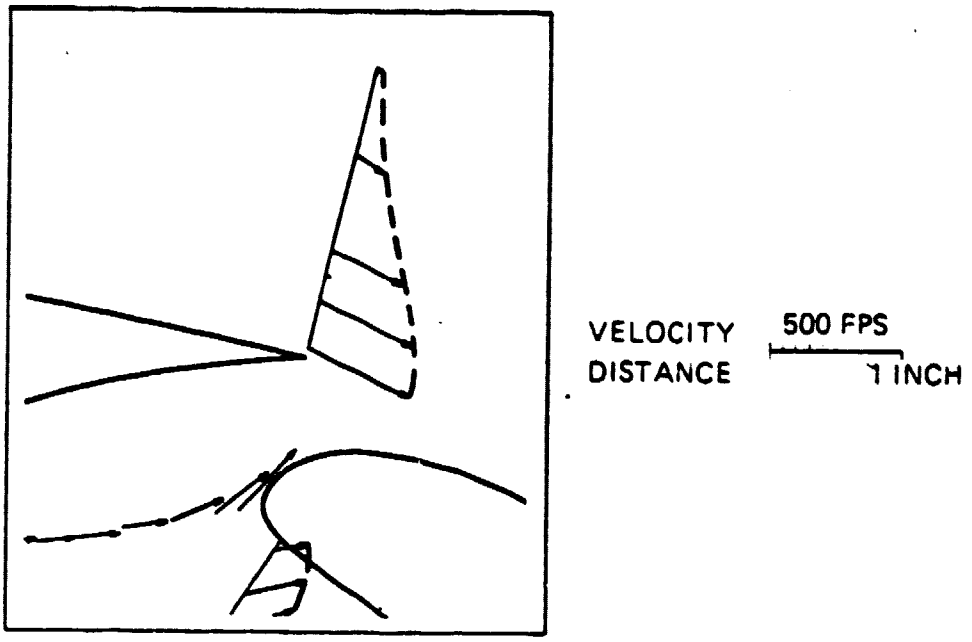

Figure 6–8. Velocities at the trailing edge of the cove at the nozzle centerline at a pressure ratio of 1.2

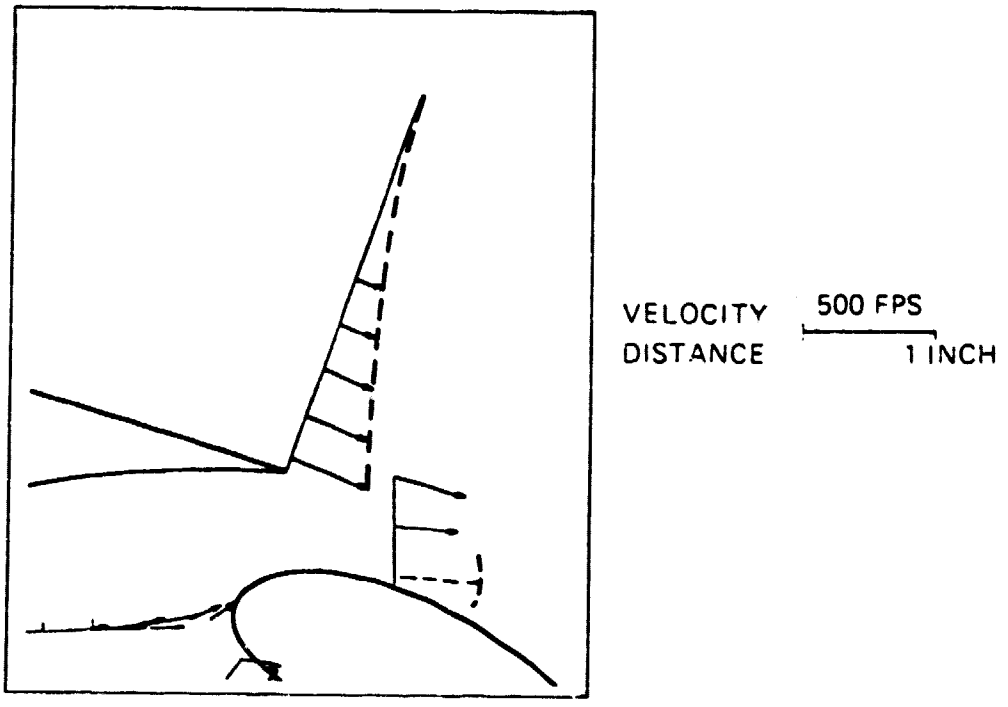

Figure 6–9. Velocities at the trailing edge of the cove at wing station 29.93 inches at a pressure ratio of 1.2

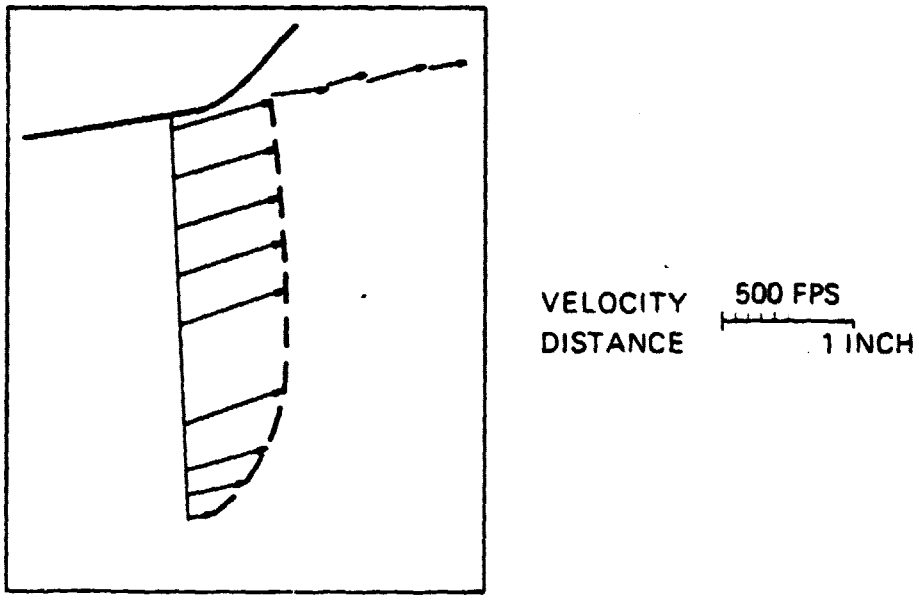

Figure 6–10. Velocities on the lower surface upstream of the wing cove at the nozzle centerline

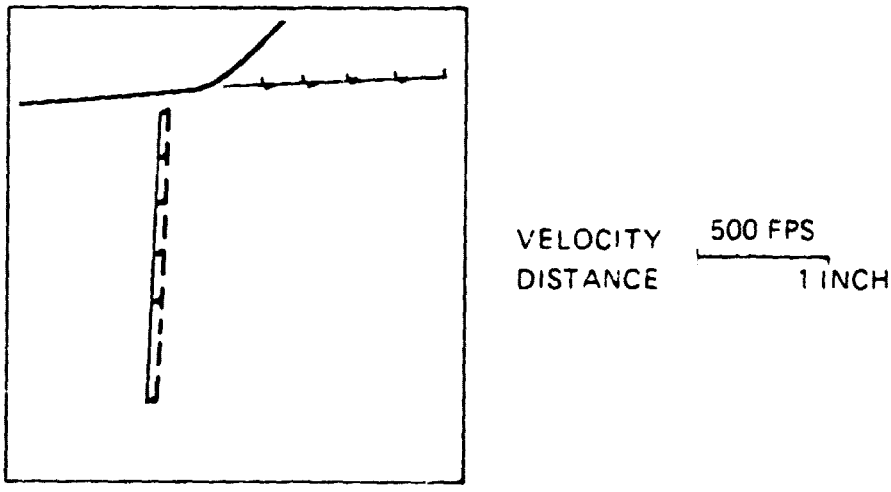

Figure 6–11. Velocities on the lower surface upstream of the wing cove at wing station 29.93 inches

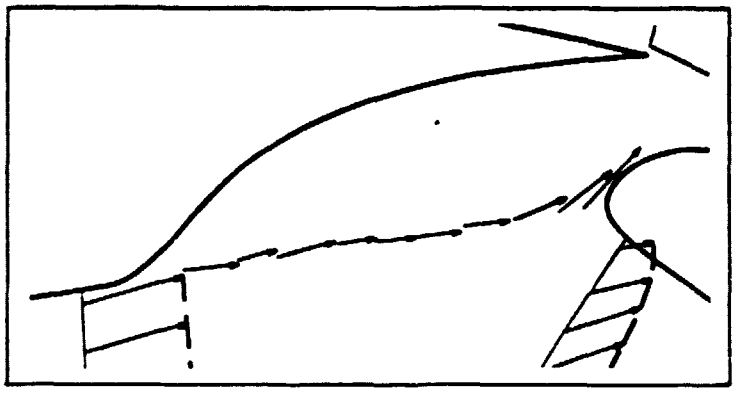

Figure 6–12. Wing cove inlet flow at the nozzle centerline

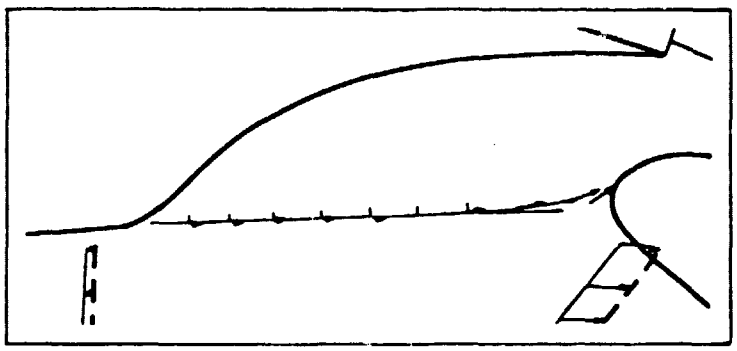

Figure 6–13. Wing cove inlet flow at wing station 29.93 inches

both locations the flow traverses 2 inches of the gap without turning, and is within 0.5 inch of the flap before it turns into the wing cove. At the outboard location the velocities at the cove are less than 80 fps, compared to the roughly 300-fps velocities at the nozzle centerline.

This velocity profile supports the flow separation deduced from the pressures measured in the wing cove. It also suggests that the wing cove is not shaped properly for the flow to be established in the cove.

The stagnation point on the flap probably occurs just under the leading edge between this traversing line and the traversing station normal to the flap just aft of the nose radius tangency point.

6.2.4 Flow over the lower surface of the first flap. – The most significant features of the flow across the lower surface of the flap are the large flow angularities into the flap surface at all locations of the split film probe, particularly along the nozzle centerline (Figure 6-14). Although such a flow could occur in the vicinity of the stagnation point, the large flow angularities away from the surface and at the rear of the flap cannot be justified on the basis of two-dimensional flow. However, if there is a significant spanwise flow outward from the centerline of the nozzle, especially close to the surface, then these flow angularities are consistent with the mass flow requirements.

The velocity profile at wing station 29.93 (Figure 6-15) also shows these flow angularities toward the surface, although not as large as at the centerline of the nozzle.

The magnitude of the velocities at wing station 29.93 (outboard station) at the front of the flap is larger than those measured at the lower surface of the wing upstream of the cove. Because of the very low velocities upstream of the cove in the chordwise direction, this increase in velocity is thought to be the result of spanwise flow outward from the centerline of the nozzle.

6.2.5 Inlet flow to the second slot. – Because of the large flow toward the lower surface of the first flap, the lower surface flow does not appear to be turned ahead of the entrance into the second slot. Thus, the flow is nearly aligned in the direction of the inlet to the second slot and a large mass flow does occur into the slot (Figures 6-16 and 6-17). The velocity at the lower surface of the flap is nearly tangent to the entrance surface and the slot flow can be assumed to be fully attached.

The velocities into the slot are nearly uniform, although the velocity profiles upstream are not.

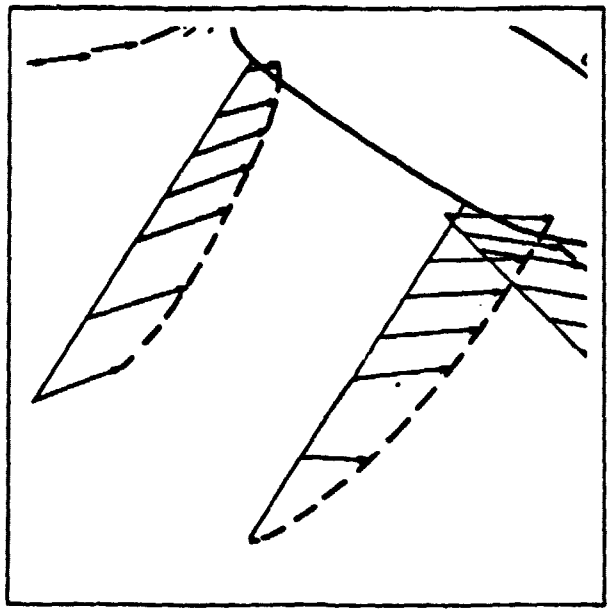

Figure 6–14. Flow over the lower surface of the first flap at the nozzle centerline

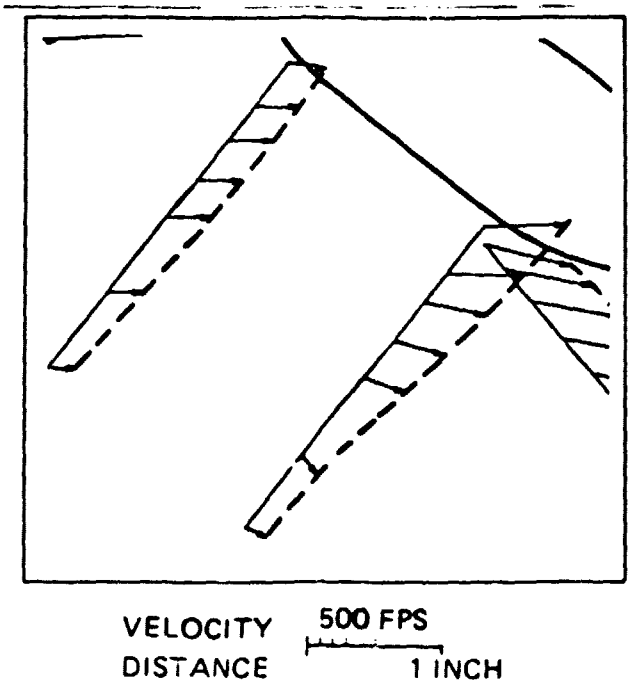

Figure 6–15. Flow over the lower surface of the first flap at using station 29.93 inches

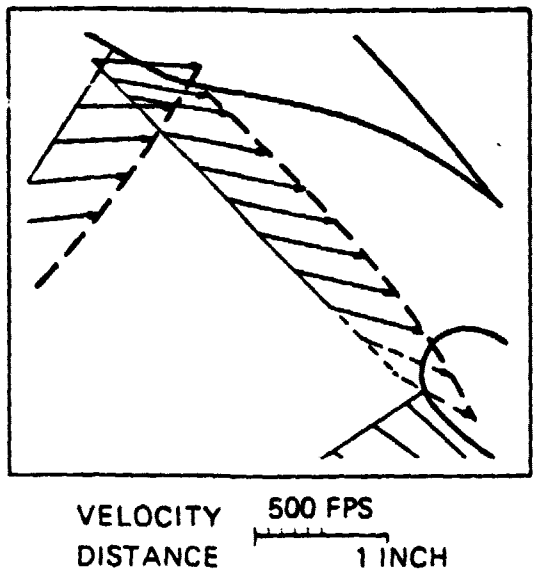

Figure 6–16. Inlet flow to the second slot at the nozzle centerline

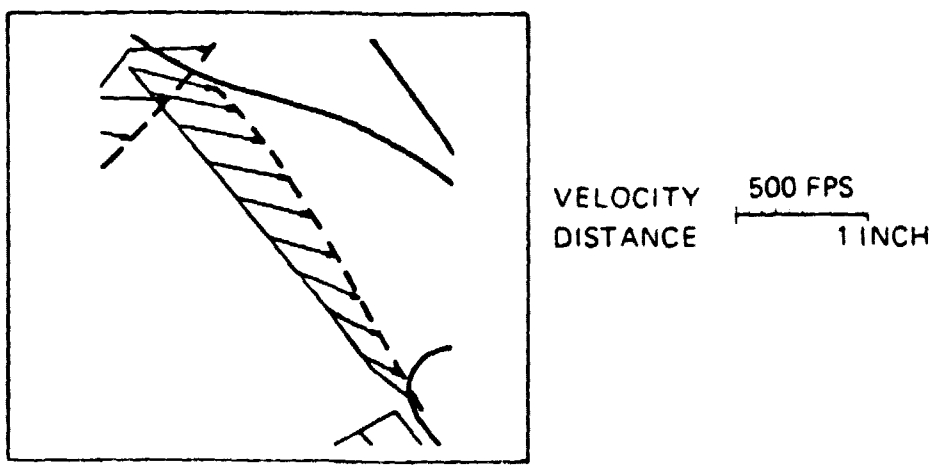

Figure 6–17. Inlet flow to the second slot at wing station 29.93 inches

6.2.6. Flow over the upper surface of the flaps. – The velocity profiles over the flaps indicate that the jet flow gradually entrains the ambient air (Figures 6–18 and 6–19). The influx of momentum from the flow through the slots is also evident in the buildup of the momentum downstream of each slot.

A significant flow phenomenon occurs on the second flap segment, downstream of the slot. The flow at the surface (0.06 inch above the surface) is tangent to the surface. However, the flow 0.3 to 0.5 inch from the surface is angled down toward the surface; the angularity away from the surfaces is less. This characteristic may be associated with the mixing between parallel jets where the low-momentum flow is induced toward the flow with the larger momentum. This angularity increases when the differences between the two velocities increase. Without study of an analytical flow model, it is difficult to ascertain that the value of flow angularity observed (approximately 15 degrees maximum) can be fully accounted for by this postulated reaction to a nearby shear flow with higher velocity.

6.3 Total Pressure Survey

The data from the miniature Kiel probe survey have been corrected for the flow angularity measured by the split film probe. This correction is defined as

$$K = \frac{P_T - P_o}{\frac{1}{2} \rho U^2}$$

where P_T = total pressure measured by the Kiel probe
P_o = true total pressure
ρ = local density
U = local velocity.

The correction factor K is a function of the flow angularity θ and is dependent on the geometry of the probe. For most of the flap flow measurements reported here, the flow angles are in the quadrant described by the probe tip axis and the stem, requiring corrections as indicated by Figure 6–20. Where the flow angularities observed in the test are in the quadrant beyond the stem and probe, these angles are less than 40 degrees and the manufacturer's calibration indicates no correction is required.

Data for the United Sensors Kiel probe used for this test were available only up to 48 degrees, the point circled in Figure 6–20 on the solid line. It has been necessary to extrapolate a correction curve for use beyond 48 degrees and this was done as follows. The other two lines were obtained from references 2 and 3. The dashed line from reference 2 is from NACA TN2530. The second datum is obtained from the equation given in reference 3:

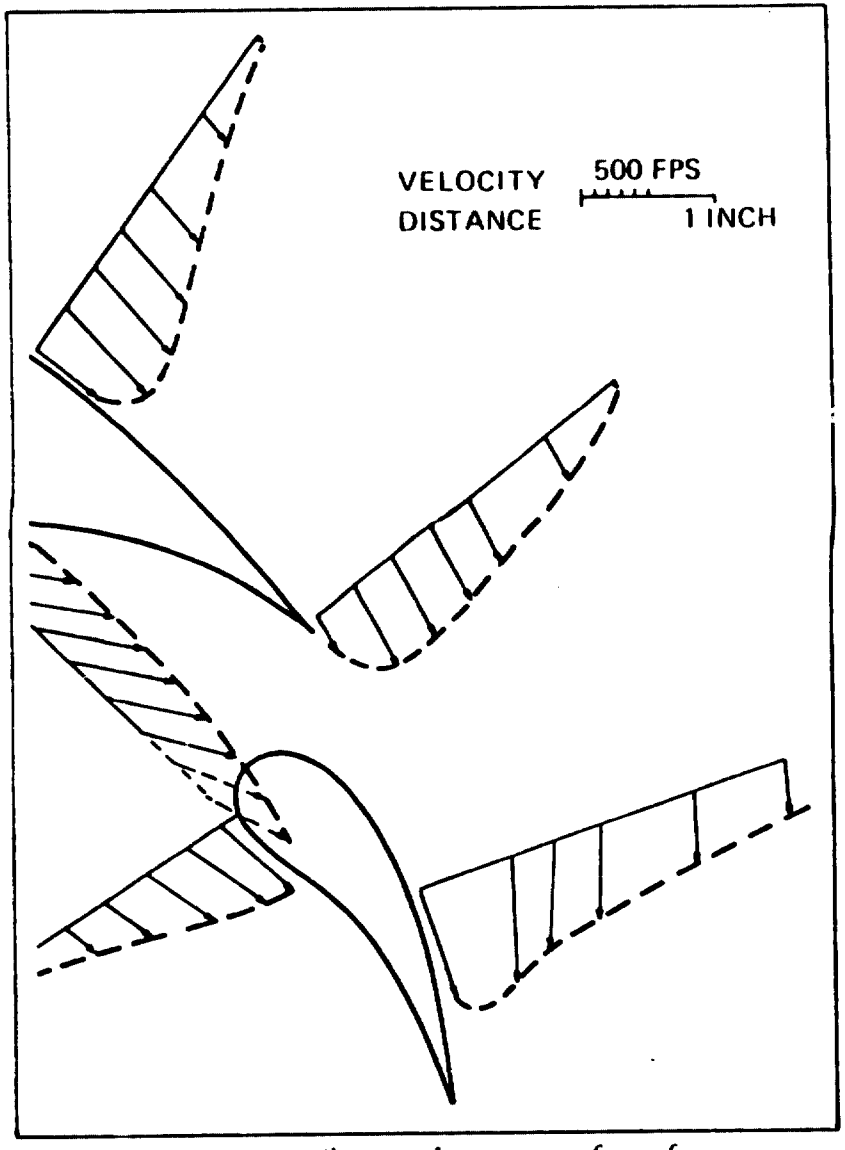

Figure 6–18. Flow on the upper surface of the flaps at the nozzle centerline

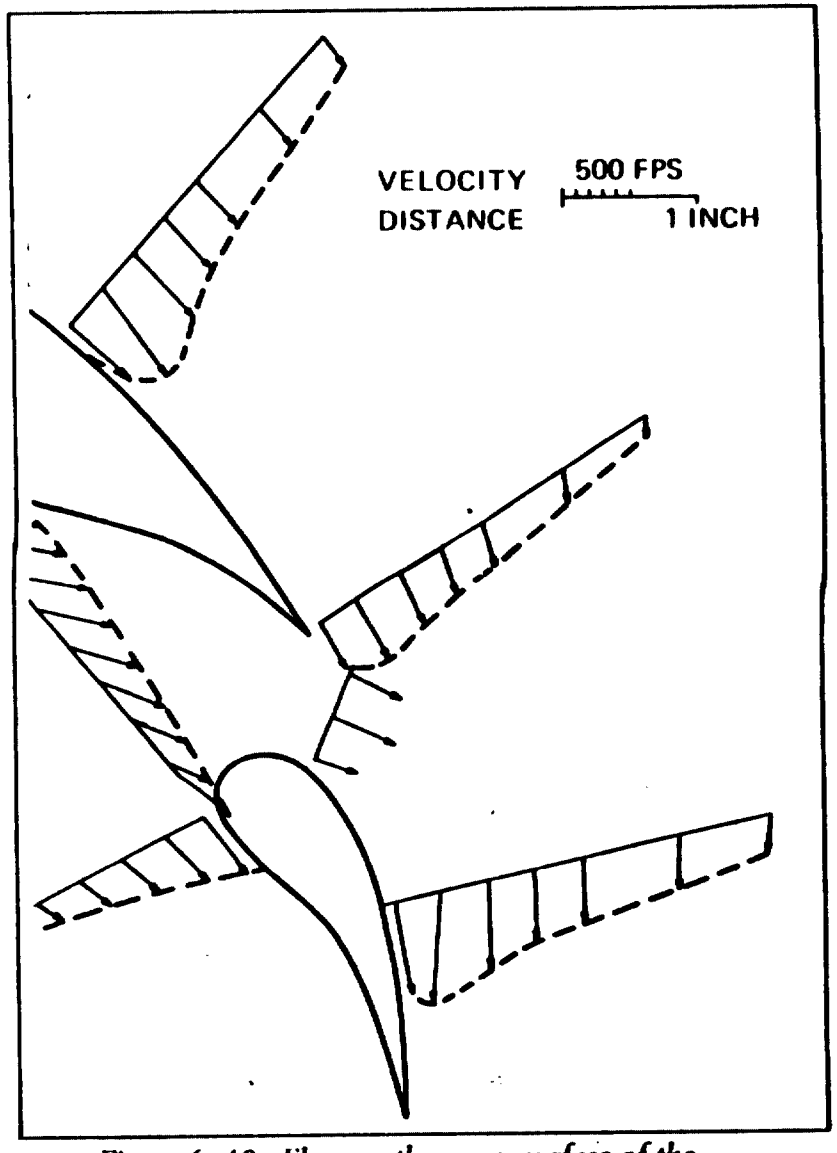

Figure 6–19. Flow on the upper surface of the flaps at wing station 29.93 inches

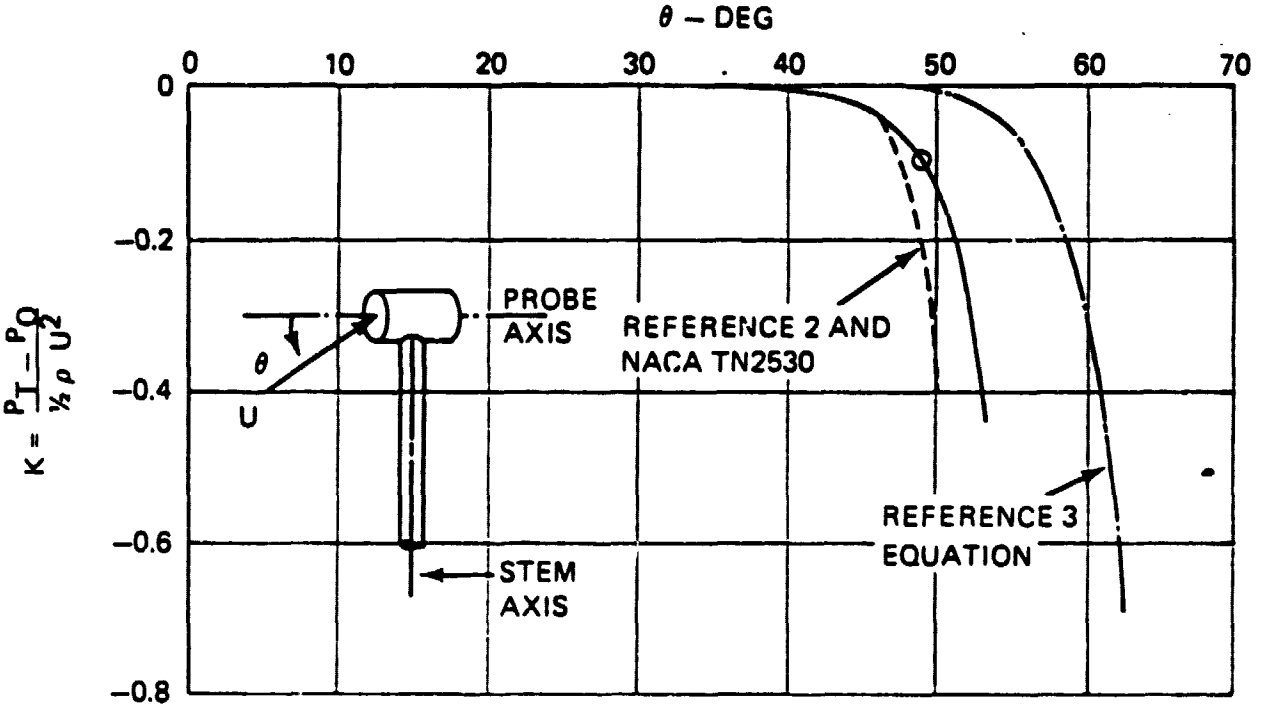

Figure 6–20. Kiel probe calibration

$$P_T - P_L = \tfrac{1}{2} \rho U^2 (1 - K (\sin^2 \theta)^m),$$

where P_T = measured static pressure

θ = flow angularity

K = 25

m = 15

P_L = local static pressure.

When this equation is rearranged it becomes

$$\frac{P_T - P_o}{\tfrac{1}{2} \rho U^2} = 25 \sin^{30} \theta,$$

and the right side is equivalent to the correction shown in Figure 6–20.

The general shapes of the available data after the break are similar, the principal differences being the shapes of the break and the points prior to the break. The data for the United Sensors Kiel probe are similar to the NACA data before the break; however, the knee of the break is similar to that of the reference 3 equation. The data were extrapolated to 53 degrees, preserving the initial shape of the break and roughly intermediate to the two available data curves for angles greater than 48 degrees.

The total pressures in psia at each of the measuring stations have been added as scalar values at the end of each of the velocity vectors (Figures 6-21 and 6-22). Each profile is a separate run, and between runs a variation of total pressure in the nacelles of up to 0.20 psia was observed. These values are noted on the profiles so that apparent streamwise variation in total pressure may be analyzed consistently.

The chordwise changes of the total pressure along the nozzle centerline of the upper surface show that the total pressures are generally decreasing in the downstream direction. On the lower surface of the first flap the total pressures measured at the aft stations are greater than those measured just upstream at the leading edge of the flap. The differences in the total pressure measured in the pod for these curves are essentially the same, i.e., 17.78 psia and 17.76 psia, and cannot be the reason for the observed increase in the total pressure. The possible flow irregularities considered under the discussion of the flow angularities in this region can be the mechanism for introducing the higher total pressure air found upstream and further from the surface into this region close to the surface. However, all such flow irregularities may be expected to increase losses in the flow and reduce the thrust recovery factor.

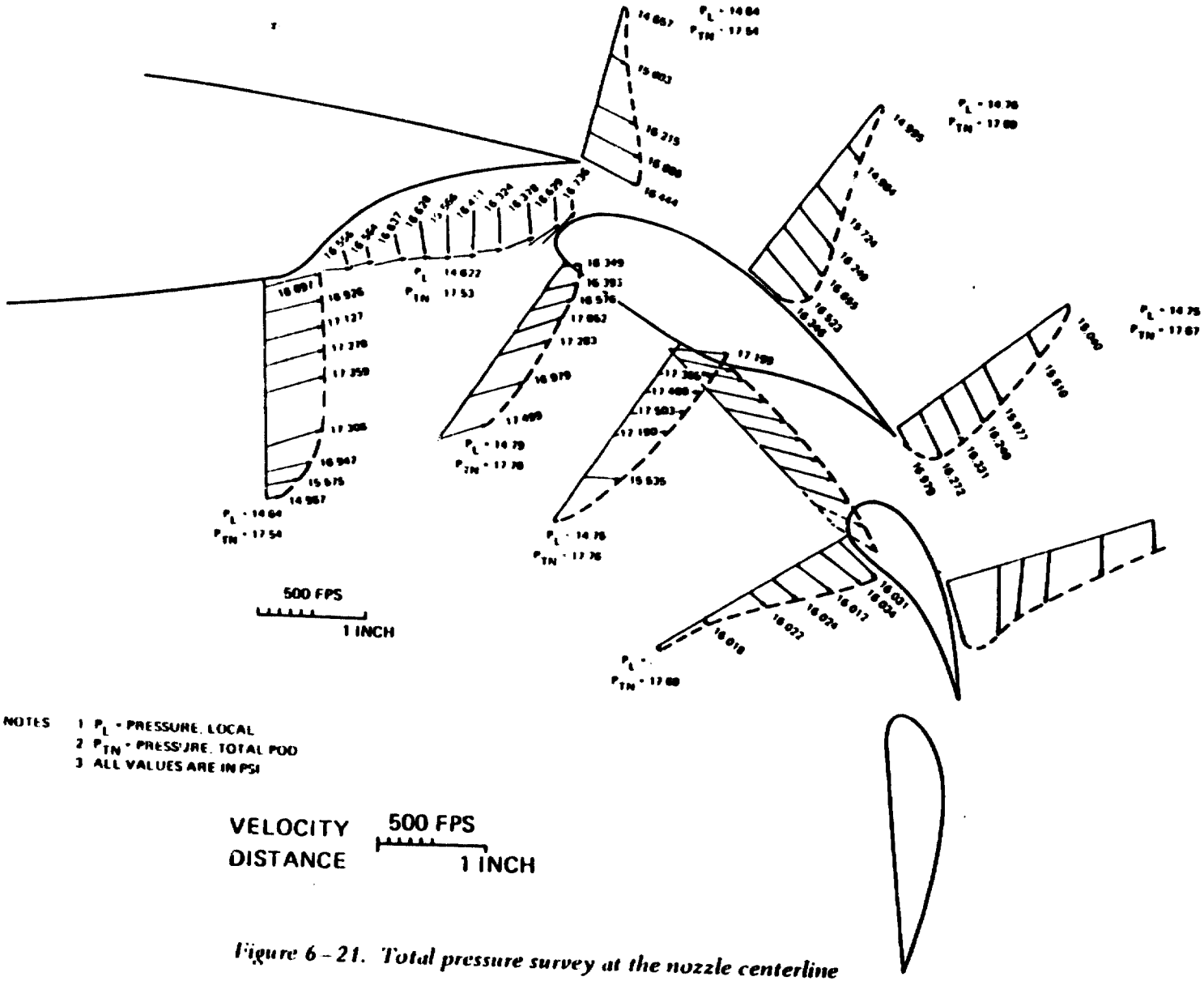

Figure 6 – 21. Total pressure survey at the nozzle centerline

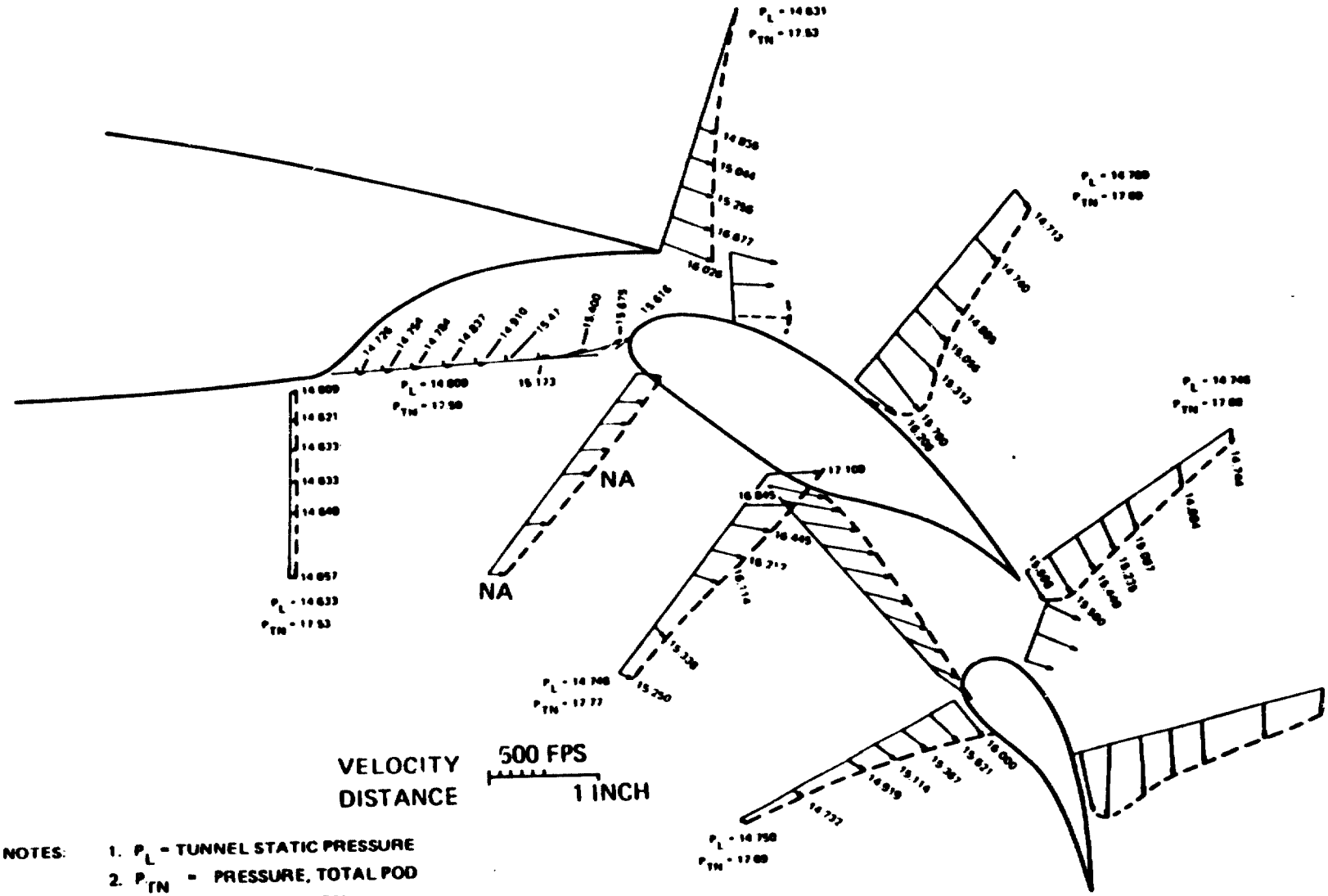

Figure 6–22. Total pressure survey at wing station 29.93 inches

7.0 INTERPRETATION OF THE DATA

The flow patterns discussed in Section 6 suggest that a number of flow phenomena occur, some of which were anticipated while others were not, and that the magnitude of some of the latter had a profound effect on the testing. The principle concern of the data interpretation has dealt with the flow pattern on the lower surface of the first flap element.

7.1 Flap Cove Flow

The flow separation in the wing cove is substantiated by both the surface pressure measurements and the velocity measurements into the cove. The size of the separation pocket is shown by the distance along the cove entrance along which the flow is aligned with the entrance, or underside of the wing. This area is greater than the flow patterns observed on other, unblown flapped wings. Reference 4 states that slotted flaps can operate efficiently when the local separation is sufficiently small and controlled so that the flow can turn into the slot and the flow remains attached to the upper surface of the flap. The separation found on the CSB system is complete in the sense that it covers nearly three-quarters of the entrance at both the nozzle centerline and the outboard position at wing station 29.93 inches. The velocities approaching the inlet to the slot and along the slot entrance at the outboard station are less than 100 fps.

Additionally, the pressure data show that the separated region is changed when the pressure ratio is increased and there is a loss of venturi effect at the cove trailing edge and leading edge of the first flap segment.

To reduce the losses in the present design of the cove, the cove inlet should be redesigned. Potentially, the losses may be reduced by sealing the exit from the cove, or a hinged flap can be installed so that no flow takes place between the wing and the flap.

The flow angularities under the first flap, from the flap surface outward, cannot be explained on the basis of two-dimensional flow. On the basis of the measured velocities at the nozzle centerline, the stagnation point must be located as shown schematically in Figure 7-1A. Although the flow around the leading-edge radius of the flap and into the cove can be deduced for this stagnation point, the flow angularity on the under surface of the flap cannot coincide with the measured direction. If the stagnation point is moved further aft to justify the flow on the under surface, Figure 7-1B, the flow direction measured adjacent to the leading edge along the entrance line cannot be consistent with the flow around the leading edge. These observations are also applicable to the flow patterns measured at the outboard survey at wing station 29.93 inches. The two-dimensional concepts must be replaced by the probability of three-dimensional flow.

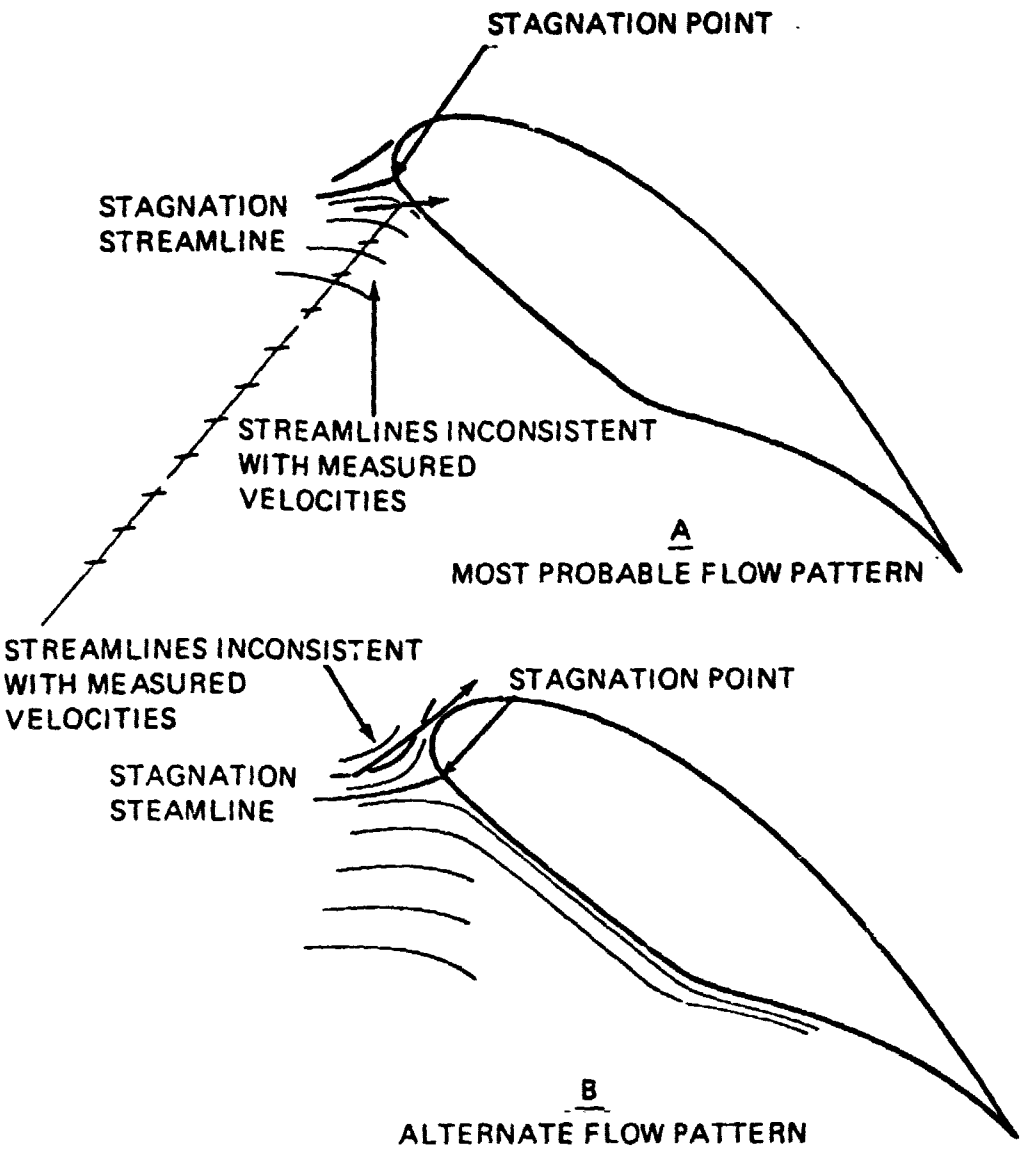

Figure 7–1. Two possible flow patterns around the leading edge of the first flap based on flow measurements

Additional arguments to support the three-dimensional nature of the flow can be deduced from the volumetric flow rates obtained for a unit span width at each of the stations by integrating the velocity profiles (Figures 7–2 and 7–3). Reference to volumetric flow rates in the following sections refers to flow rate per unit span. If the flow is two-dimensional, continuity is not satisfied along the lower surface of the flaps. Also, referring to the flow under the first flap segment, the increase in the total pressure from the front of the flap to the rear of the flap cannot be explained on the basis of two-dimensional flow.

The following discussion can explain what seem to be inconsistencies in the flow rates on the basis of the postulated lateral spreading. The higher total-pressure flow found upstream and away from the surface must be transported closer to the surface downstream to be consistent with measured data. This would suggest that the upstream flow close to the surface has spread laterally and thinned, bringing the higher energy flow in closer to the downstream surfaces. Mixing also can convect fluid with higher total energy into a region which should have a lower total pressure on the basis of steady flow.

This discussion on lateral spreading is intended to be illustrative and is not intended to be quantitative. Assume that we can construct a control surface which consists of streamlines of the flow so that flow does not take place across the control surface. Assume that lateral spreading of the flow occurs.

First, consider the case where the flow areas consist of only upstream and downstream stations. All the other surfaces in Figure 7–4 are streamline surfaces. Even though the volumetric flow rate along the centerline increases from 60 ft^3/sec/ft to 68 ft^3/sec/ft and the flow spreads and the flow rate drops off laterally, continuity is still satisfied.

This argument can be expanded to include three control stations through which mass flow can occur, i.e., across a slot entrance, Figure 7–5. The control surface for the incoming flow is the left surface and the two surfaces at the right side can represent the flow into the slot and the downstream control surface. Although the flow rates along the centerline are not consistent in themselves, continuity is preserved when the lateral flow is considered.

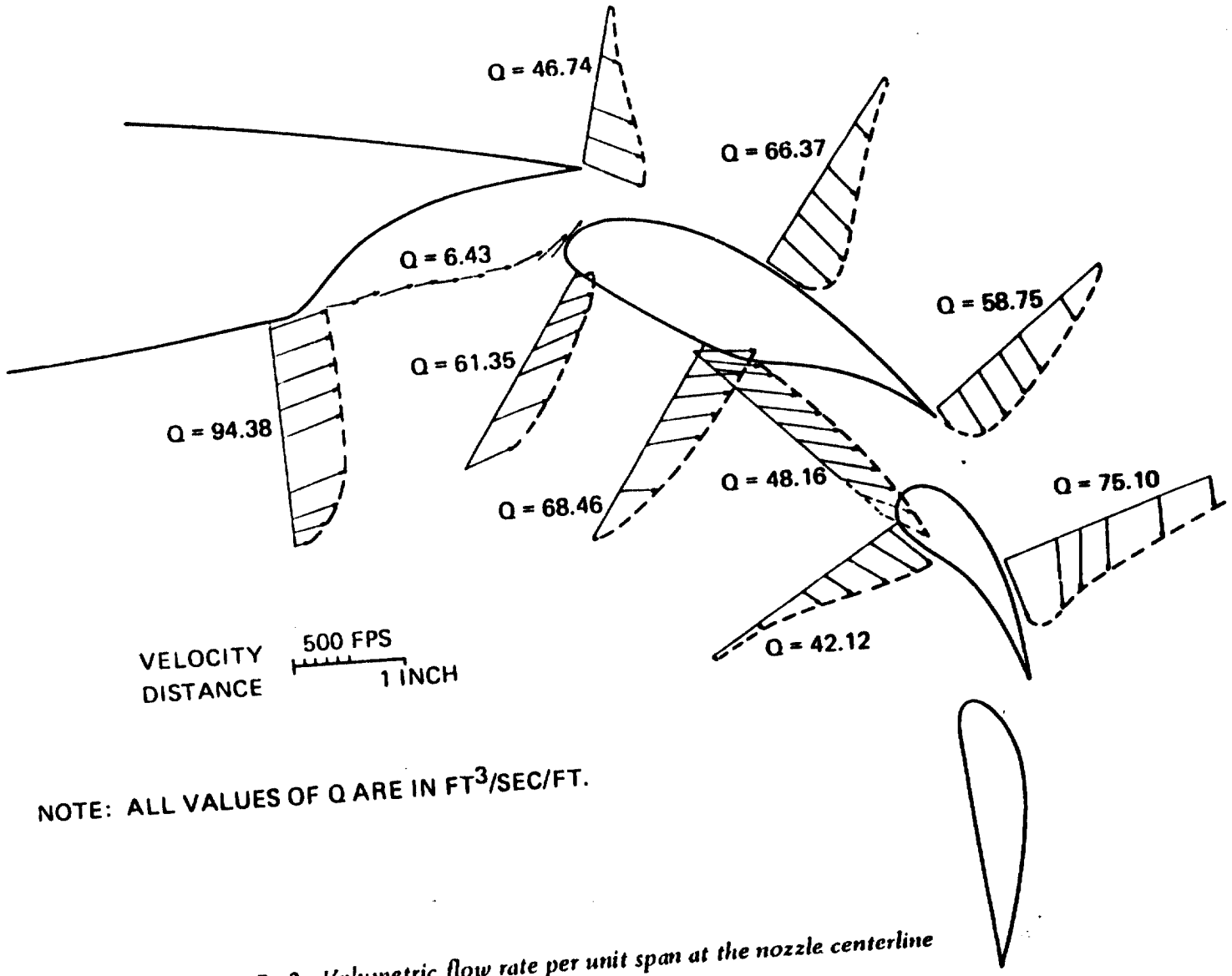

Figure 7–2. Volumetric flow rate per unit span at the nozzle centerline

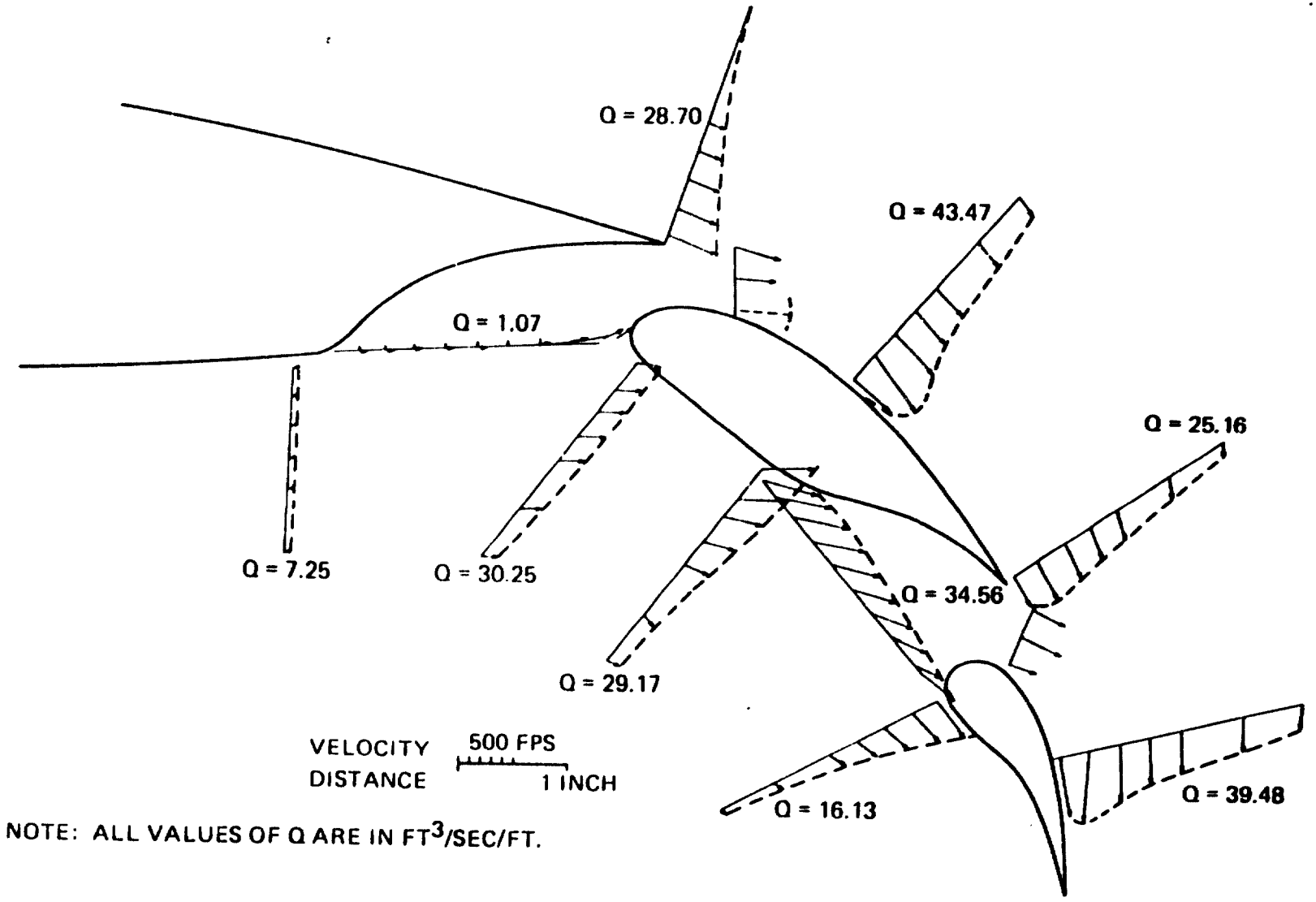

Figure 7- 3. Volumetric flow rate per unit span at wing station 29.93 inches

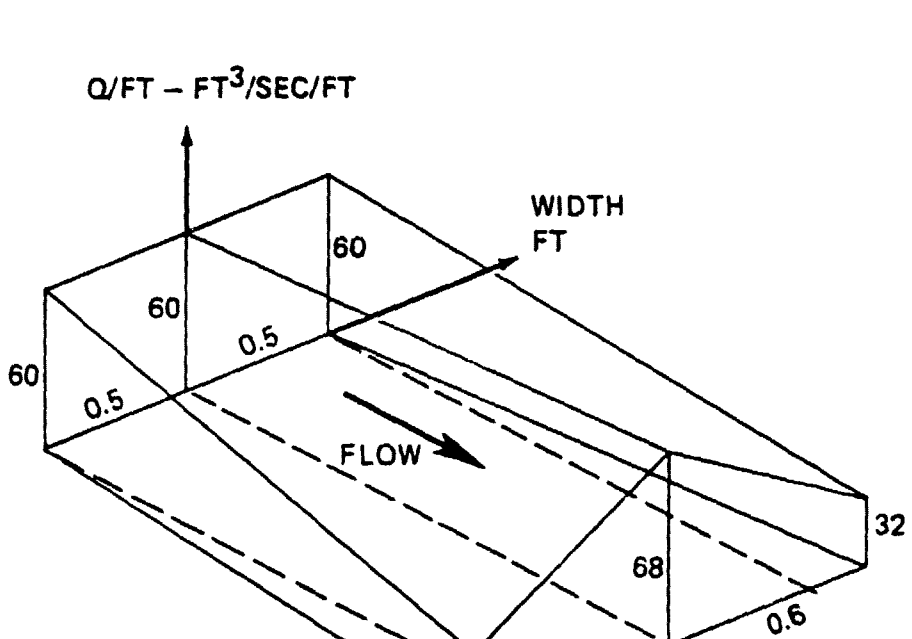

Figure 7–4. Spreading of lower-surface flow

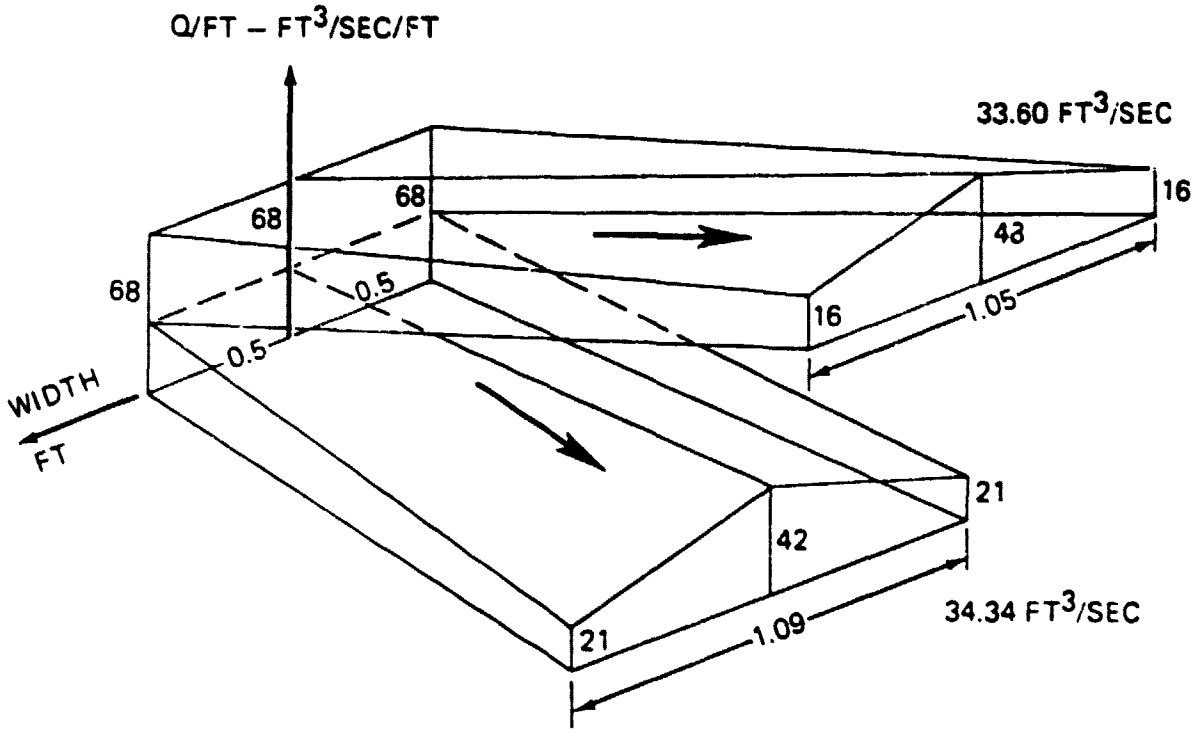

Figure 7–5. Spreading of upper- and lower-surface flows

8.0 RECOMMENDATIONS

The data presented in the preceding sections indicate that flow over the CSB system tested in the static condition has significant three-dimensional characteristics. The degree to which this three-dimensionality affected the flow from the nozzle over the flaps was not evident before this test. The lateral spreading had been qualitatively observed by the china clay studies during the tests of reference 1. Limited tuft studies during those tests also showed the vortex flow in the mixing regions at the periphery of the jet. However, those visualization methods did not indicate the distribution of the airflow through the flap gaps and over the flap segments and the amount of spanwise flow, as did the measurements taken during this test.

It appears that the extent of lateral flow in terms of angle, velocity, and amount of air exceeded the boundaries of planned instrumentation in terms of additional spanwise stations and lateral flow vector measurements. The vertical flow vector measurements which were taken indicated higher angularities closer to the surface than had been expected. For these reasons, a more thorough experimental study of the CSB flow should include a broader dimensional boundary for flow field measurement and the addition of lateral flow vector measurements.

Because of the lateral flow and the indicated extent of the induced flow, the measurements at intermediate spanwise stations are required to determine the source of the fluid with the higher total pressure. Additionally, the traversing distance should have been larger to reach the boundary of the nozzle flow and any induced flow. All vertical flow must be contained within this measuring volume.

Although the redistribution of the volumetric flow can be accounted for by lateral flow spreading, the apparent transport of locally high total pressures at the survey stations under the first flap element requires a mechanism other than spreading. Vortex flow is a possible mechanism. If such a flow does exist, it will be a source of loss other than that due to friction, which is inherent in the CSB concept.

There is indication from reference 1 that changes in the first flap gap did not appreciably affect the thrust recovery, and observations from this test indicate that there is little flow through the fixed flap gap. There is indication of a large separated pocket of flow in the cove. From these observations it appears that either the flap cove should be redesigned to achieve the desired slot action over the first flap segment and thereby to determine if the thrust recovery improves, or to seal and fair over the cove gap and assess any changes in thrust recovery. There is indication that the flow on the upper surface of the flap is reenergized primarily by flow from the second slot rather than the first, and that flow through the first slot may be unnecessary for turning the flow over the first flap and achieving the thrust recovery.

Because of the adverse flow conditions into the wing cove, it would be convenient to suggest that the cove be eliminated and/or a flapped hinge installed.

The following changes to the model are suggested to improve the flow pattern and the thrust recovery:

1. The cove inlet should be either made more gradual to keep the flow attached and reduce the blocking effect of the separated region in the cove, or the inlet contour can be modified to achieve a separated region with a shape which will reattach the flow into the wing cove. This change should decrease the losses across and through the first slot, and keep the flow on the upper surface of the first flap element.

2. The longer first flap element, as in Configuration B over Configuration A as investigated in reference 1, is advantageous to direct the higher momentum flow under the first flap. However, the flap should be redesigned as a turning element with a concave lower surface in place of the flat surface. This may correct the flow problems such as the angularities noted in the previous discussions.

9.0 REFERENCES

1. Schoen, Allen H.; Kolesar, Charles E.; and Schaeffer, Edward G.: Static, Noise, and Transition Tests of a Combined-Surface-Blowing V/STOL Lift/Propulsion System. Boeing Vertol Company, Philadelphia, Pennsylvania; NASA CR-151954, National Aeronautics and Space Administration, Ames Research Center, Moffett Field, California, April 1977.

2. Dean, R. C., Jr.: Aerodynamic Measurements. Gas Turbine Laboratory, Massachusetts Institute of Technology, Cambridge, Massachusetts, 1953.

3. Becker, H. A.: and Brown, A.: Response of Pitot Probe in Turbulent Streams. Journal of Fluid Mechanics, Volume 62, page 85.

4. Hoerner, S. F.: and Borst, H. V.: Fluid Dynamic Lift. Fluid Dynamics, Bricktown, New Jersey, 1975.